JOURNAL OF ENGINEERING RESEARCH & SCIENCES

JENRS

www.jenrs.com
ISSN: 2831-4085

Volume 3 Issue 4
April 2024

EDITORIAL BOARD

Editor-in-Chief

Editorial Board Members

Editorial

In an era characterized by rapid technological advancement and interdisciplinary collaboration, research endeavours continually push the boundaries of knowledge across diverse domains. The collection of these 4 papers featured in this issue embodies this spirit of innovation, offering novel insights and methodologies that address pressing challenges in fields ranging from biomechanics to healthcare and environmental science. From the development of modular estimators for precise joint motion analysis to the exploration of computational models for disease comorbidity identification, each paper reflects a commitment to advancing understanding and driving practical applications. As we delve into the intricacies of these studies, we embark on a journey through the frontiers of research, where curiosity, creativity, and cutting-edge technology converge to shape the future of science and society.

Estimating the intricate movements of human joints, particularly with high accuracy, poses a significant challenge. In this paper, the authors present a novel modular estimator tailored for estimating elbow joint motion. Notably, this estimator's modularity facilitates its adaptation for other joints, promising versatility across applications. The methodology integrates surface Electromyographic (sEMG) signals and motion capture data, enabling precise estimation of angular displacement and movement direction during elbow flexion and extension. Impressively, the classifier achieved estimation accuracies ranging from 80% to 90%, showcasing its potential for various Human-Machine Interface (HMI) applications [1].

Assessment methodologies profoundly influence student learning outcomes and experiences. This paper explores the efficacy of e-assessment via the Halomda educational platform in improving student performance and enriching learning experiences. Integration of ChatGPT with math exploration tools further enhances learning both in-class and remotely, while supporting educators in their assessment and feedback processes. The study's findings not only demonstrate improved student performance on final exams but also highlight a strong correlation between exam scores and continuous assessment grades, emphasizing the importance of holistic assessment approaches [2].

The stability of riverbanks in riparian zones is critical for environmental preservation and infrastructure development. This research presents a comprehensive investigation into riverbank slope stability, particularly along the Yellow River in China. By integrating empirical data with numerical analysis, the study unveils the intricate interplay of factors such as water level fluctuations, precipitation, and vegetation on slope stability. Notably, vegetation emerges as a significant factor in stabilizing riverbanks, especially during precipitation events. While acknowledging methodological limitations, the study underscores the relevance of these findings for informed decision-making in riverbank protection and infrastructure planning [3].

The COVID-19 pandemic has underscored the importance of understanding disease comorbidities for effective patient management. This paper presents a computational model designed to identify comorbidities associated with COVID-19 using transcriptome datasets. Through gene expression analysis and comprehensive data mining, the model reveals correlations between COVID-19 and various diseases, including acute myelocytic leukemia, urinary tract cancer, and diabetes mellitus. Notably, the model's insights pave the way for potential shared treatment strategies, offering prospects for improved patient care [4].

These research papers contribute significantly to their respective fields, showcasing innovative methodologies and yielding valuable insights. From advancements in joint motion estimation to the elucidation of disease comorbidities, each study addresses critical challenges with rigor and ingenuity. As we navigate an increasingly complex world,

interdisciplinary collaborations and technological innovations are paramount for driving progress and enhancing human well-being.

References:

[1] A. Y. Al-Maliki, K. Iqbal, G. White, “Estimation of Elbow Joint Movement Using ANN-Based Softmax Classifier,” *Journal of Engineering Research and Sciences*, vol. 3, no. 4, pp. 1–9, 2024, doi:10.55708/js0304001.

[2] P. Slobodsky, M. Durcheva, “Comprehensive E-learning of Mathematics using the Halomda Platform enhanced with AI tools,” *Journal of Engineering Research and Sciences*, vol. 3, no. 4, pp. 10–19, 2024, doi:10.55708/js0304002.

[3] M.T. Ahsan, J.-P. Wang, A. Dadda, “Numerical Analysis of Riverbank Slope Stability Considering Rainfall, Vegetation and Water Level Fluctuation,” *Journal of Engineering Research and Sciences*, vol. 3, no. 4, pp. 20–31, 2024, doi:10.55708/js0304003.

[4] S.B. Sen Omit, M. Mohiuddin, S. Akhter, Md.H. Imam, A.K.M.M.K. Habib, S.M.M. Hossain, N.K. Podder, “Computational and Bioinformatics Approaches for Identifying Comorbidities of COVID-19 Using Transcriptomic Data,” *Journal of Engineering Research and Sciences*, vol. 3, no. 4, pp. 32–41, 2024, doi:10.55708/js0304004.

Editor-in-chief

Prof. Paul Andrew

JOURNAL OF ENGINEERING RESEARCH AND SCIENCES

Volume 3 Issue 4 April 2024

CONTENTS

Received: 21 January, 2024, Revised: 22 March, 2024, Accepted: 23 March, 2024, Online: 16 April, 2024

DOI: https://doi.org/10.55708/js0304001

Estimation of Elbow Joint Movement Using ANN-Based Softmax Classifier

Abdullah Y. Al-Maliki [*,1], **Kamran Iqbal** [1], **Gannon White** [2]

[1]Department of Electrical and Computer Engineering, University of Arkansas at Little Rock, Little Rock, 72204, USA

[2]Department of Kinesiology, Colorado Mesa University, Grand Junction, 81501, USA

*Corresponding author: Dr. Abdullah Al-Maliki, ayalmaliki@gmail.com

ABSTRACT: Estimating the natural voluntary movement of human joints in its entirety is a challenging problem especially when high accuracy is desired. In this paper, we build a modular estimator to estimate the elbow joint motion including angular displacement and direction. Being modular, this estimator can be scaled for application to other joints. We collected surface Electromyographic (sEMG) signals and motion capture data from healthy participants while performing elbow flexion and extension in different arm positions and at different effort levels. We preprocessed the sEMG signals, extracted features array, and used it to train an ANN-based Softmax classifier to estimate the angular displacement and movement direction. When compared against the motion cap-ture data, the classifier achieved estimation accuracy ranging from 80% to 90% with a resolution of 5°, which translates into Pear-son Correlation Coefficient (PCC) ranging from 0.91 to 0.95. Such high PCC values in mimicking the voluntary movement of the upper limb may help toward building intuitive prostheses, exoskeletons, remote-controlled robotic arms, and other Human Ma-chine Interface (HMI) applications.

KEYWORDS: Elbow Angle Estimation, ANN, Softmax Classifier, sEMG, Signal Processing

1. Introduction and Literature Review

An Individual's intent to perform any physical movement that involves the contraction of skeletal muscles can be estimated by analyzing the corresponding muscles' electromyography (EMG) signal [1,2]. An EMG signal is the electrical manifestation of the neuromuscular activation associated with a muscle contraction [3]. EMG signals are characterized as a stochastic and nonlinear signal due to a large number of motor units and their different firing rates, as it carries the brain command to create a muscle contraction [4]. Since the EMG signal has a low signal-to-noise ratio in addition to its stochastic nature, it is hard to fully utilize the information embedded in it with high accuracy without implementing various filtering, dimension reduction, and/or pattern recognition techniques [4,5]. EMG can be measured by using one of two methods; surface EMG or sEMG and intramuscular EMG. sEMG is measured on the skin above the muscle of interest using an electrode to measure the muscle's electrical activity i.e. EMG signal [6]; therefore, this technique is categorized as noninvasive [6,7]. Intramuscular EMG, on the other hand, is measured from within the muscle of interest by inserting thin metal electrodes into the muscle and referenced to the surface electrode placed above the muscle [8]. Consequently, it requires more caution than sEMG to perform and it is considered an invasive procedure [9,10]. As a result, sEMG is the dominant method to study how the human body controls skeletal muscles as it is safer, easier to perform, and can be implemented in end products with less complexity [7,10].

This work focuses on estimating the direction and angular displacement of the elbow's joint flexion and extension movement using the information embedded within sEMG data of the related muscles. Below we mention some of the related research addressing the same problem using various methods. The authors trained an Artificial Neural Network (ANN) to estimate the upper limb joint angles from related muscles' sEMG data, in their experiment setup the upper arm was held fixed at the shoulder level [11]. Their ANN was able to follow the

target angle in training data, and they showed low average Mean Square Error (MSE) for eight participants. The authors measured the upper limb joint angles, muscles EMG and set a constant load to estimate the angle-torque relation during constant muscle activation in able-bodied humans using ANN [12]. The authors showed the effectiveness of Kalman Filter in linearizing a set of twelve time-domain features. They estimated the elbow joint angle during elbow flexion with a fixed load and position which in turn increased the elbow angle estimation accuracy [13]. The authors used least squares support vector regression to estimate the knee and hip joint angles using sEMG signals [14]. Their data was from able-bodied participants performing treadmill and leg extension exercises. They were able to achieve single-digit Root Mean Square Error (RMSE) between measured and estimated joint angles in training data. The authors were able to estimate the elbow joint angle in able-bodied participants, using multiple time-delayed features of the sEMG and random forests [15]. They were able to achieve single-digit MSE but they had a fixed time window, with strictly one degree of freedom, fixed arm effort, and fixed arm orientation. The same authors from [15] used grey feature weighted least square support vector machine algorithm to estimate the elbow joint angle [16]. Similar to [15], the estimation was for one degree of freedom while the elbow was fixed on the table, and the starting angle between the forearm and the upper arm was 90°and the wrist joint was kept along the forearm and again all the movements were done with empty hand i.e. single effort level. The authors used EMG to model muscle activation with the help of a feed-forward ANN and Gaussian process to estimate the fingers' joint angles of ten able-bodied participants [17]. Their estimation involved more than one degree of freedom, but was held constant at one effort level. The authors used Radial Basis Function ANN to estimate the elbow joint angle for a flexion and extension movement in healthy participants [18]. Their experimental setup included fixed elbow location, fixed elbow orientation, and a fixed effort level. They achieved correlation coefficient values between actual and estimated angle ranging from 0.76 to 0.91 depending on the movement speed.

The above literature review shows that most, if not all, of the related research, did not account for the following factors when trying to estimate the elbow's joint movement:

1. Different limb orientation when performing the movement
2. Carried load changes between trials of the same movement
3. Movement speed variation between trials

Therefore, the goal of this work is to estimate the human elbow joint displacement and direction using sEMG signals for one degree of freedom at two different limb orientations, two different load levels, and variable movement speed, thus expanding on the previously mentioned studies. By developing such a versatile joint angle estimator, we broaden the utilization of sEMG signal data in different Human Machine Interface (HMI) application. For an instant prosthesis development has, in a way, surpassed the current limb action estimation techniques; as modern prostheses have multiple degrees of freedom, actuated by motors capable of fine movements [19], while the majority of the cur-rent literature focuses on the estimation of the limb torque during a muscle contraction and not so on the final location of the limb [19–21]. The estimator developed in this work is designed with a modular approach from the software point of view; so it can be scaled to other joints and their corresponding muscle groups, e.g., the wrist or the shoulder.

2. Elbow Joint Movement Estimation

In this section, we describe the biomechanics of the elbow joint and which muscles to focus on to estimate the elbow flexion and extension movement, we also discuss the sEMG signal characteristics and the procedure used in collecting sEMG data for this study. Then we show the methods used to preprocess this data and the building blocks of the elbow angle estimator, and by the end of this section, we show the estimation results of the developed estimator and the correlation factor between the actual and estimated elbow angles.

2.1. Elbow Joint Anatomy and Biomechanics

Healthy humans take their elbow joint function for granted, but as researchers try to tackle this joint, they realize how complicated this joint is. The elbow joint consists of and is a pathway to a lot of different types of bone structures, tissues, vessels, and fibers [22,23], however in this work we are focusing on the muscles responsible for flexing and extending the joint which can be divided into two groups [23].

1. The prime movers and heavy lifters of the forearm are [23]:
   - A. Biceps (Elbow Flexion)
   - B. Brachialis (Elbow Flexion)
   - C. Triceps (Elbow Extension)
2. The secondary movers and supporting muscles are [23]:
   - A. Brachioradialis (Elbow Flexion)
   - B. Pronator teres (Elbow Flexion)
   - C. Anconeus (Elbow Extension)

The location of the three heavy lifting muscles in number 1 above with respect to the upper limb is shown in Figure 1 [22].

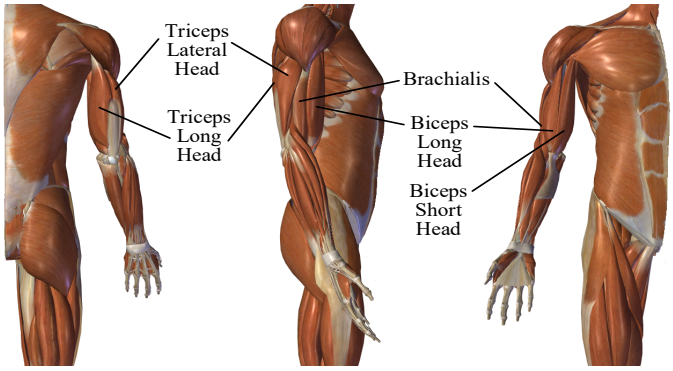

Figure 1: Shows the location of elbow joint muscles targeted in this study [22].

What is interesting is that the body utilizes the elbow muscles in a selective, highly case-dependent manner [22]. For unconstraint and unloaded forearm moving at medium speed, and when the arm is on the side of a standing hu-man, biceps, and brachialis are mainly used to raise and lower the arm, and triceps is mainly used to stabilize the elbow. This movement is known as biceps curls. And the opposite is true when the hand is raised above the shoulder and the arm is extended to the top. In this case, the triceps is mainly used to extend the arm, biceps and brachialis are used to stabilize the elbow, this movement is known as triceps extension [23].

2.2. sEMG Signal Limitations

Many researchers agree that sEMG is the most common and most feasible way to study limbs' movements and to control prosthetic limbs [24]. Nevertheless, getting useful data from the stochastic sEMG signal has its own challenges [25]. Common disadvantageous characteristics and noise sources of sEMG signal are [26–30]:

1. sEMG signal is Quasi-Random in nature
2. High noise to signal ratio (NSR)
3. Cross-talk noise, which can be mitigated by using smaller footprint sensors and by accurately targeting the muscles in question
4. Inherent equipment and electrode noise (can be estimated to a certain degree from resting trials of sEMG data re-cording session)
5. Inherent electromagnetic noise from the environment e.g. electric power, (part of which can be figured out from the power line frequency, 60 Hz in the USA)
6. Motion artifact noise (usually high amplitude, comparable to sEMG signal and low frequency 1-10 Hz)
7. Heartbeat artifact noise, which is usually very consistent with Electrocardiographic (ECG) signal.
8. Other biological noise sources, e.g. blood flow velocity, fat index, and skin temperature.
9. Fatigue resulting from task repetition and/or increasing the load has its toll on the sEMG signal.
10. sEMG signal distribution is highly non-Gaussian at low and high levels of force, whereas the distribution has its maximum gaussianity at the mid-level of maximum voluntary contraction (MVC). Therefore some techniques may work well at certain levels of the contraction power and fail at different levels [28].

It is obvious that most of the above-mentioned drawbacks are biological noises, some of which can be dealt with using different kinds of filters, and others will need different approaches to get more accurate data from the sEMG.

2.3. Data Collection

Since we can reflect the sEMG signal processing and classification from able-bodied to amputees with not much loss of accuracy [31,32], in this study we will only collect data from volunteer able-bodied participants. The data collection was done in accordance with the Institutional Review Board (IRB) guidelines. Our study was approved by IRB with protocol number 18-134-R1. After describing the whole procedure to the volunteers and signing the consent form, four silver/silver chloride (Ag/AgCl) electrodes were put on the muscles responsible for flexing and extending the elbow joint. The first channel was assigned to the biceps between the long-head and short-head, the second to brachialis, the third to triceps lateral, and the fourth and last channel was assigned to triceps long head. Retro-reflective markers were placed on the right arm of the participants to utilize the Vicon motion capture system to measure the elbow joint angular displacement. Noraxon TeleMyo Direct Transmission System (Noraxon USA Inc) was used to record the sEMG and motion data. The sEMG sampling frequency was set to 1500 Hz. Each participant was asked to perform fifteen arm flexing and extension movements at their own pace in three different arm positions:

A. The arm is relaxed by the participant side, a.k.a biceps curl movement
B. The arm abducted to shoulder height to the side of the participant, in which the elbow flexes and extends in the horizontal plane, perpendicular to the gravitational force.
C. Arm above the shoulder, i.e. overhead arm extension movement a.k.a triceps extension.

All three of the above movements were done with an empty hand and while holding a 5-pound weight (two effort levels). We also recorded sEMG data for each arm position while it's idle i.e., with no movement. Each trial lasted approximately 20 seconds which is the average time the participants took to complete 15 repetitions.

We allocate 80% of the acquired data for training the classifier and 20% for testing it. We also implement a five-fold cross-validation method on the whole data to verify the effectiveness of the classifier across all sections of the data.

2.4. Signal Preprocessing

As mentioned in Section 2.2, sEMG signal suffer from different kinds of noise; to address some of these signal imperfections, preprocessing is a must to obtain useful information out of the signal. In this case, we have implemented the following:

1. Removal of DC bias.
2. Notch filters to filter out power line fundamental and harmonic frequencies.
3. Bandpass filter allowing frequencies ranging from 30-400Hz to pass and has a low band stop frequency of 25Hz and a high band stop frequency of 450Hz.
4. Scaling up the signal by a factor of two.

2.5. Elbow Joint Motion Estimator

In this section, we design the estimator which will estimate the elbow joint's angular displacement magnitude in degrees, as well as its movement direction. Furthermore, it needs to do so while being insensitive to the elbow's angu-lar speed, orientation, or load changes.

The designed estimator is a classifier at its core, and to be more specific it is an ANN-based Softmax classifier. The softmax function is shown in (1) [33]:

$$P(c_r|x) = \begin{cases} \frac{P(x|c_r)P(c_r)}{\sum_{j=1}^{k} P(x|c_j)P(c_j)} & , (General\ Form) \\ P(c_r|x) = \frac{e^{a_r}}{\sum_{j=1}^{k} e_j^a} & , \begin{pmatrix} Normalized \\ Exponential\ form \end{pmatrix} \end{cases} \quad (1)$$

Where

$a_r = \ln\big(P(x|c_r)P(c_r)\big)$

$P(x|c_r)$ is the conditional probability of the sample x given class r and it has to satisfy the following two conditions:

$0 \le P(c_r|x) \le 1 \quad , \quad \sum_{j=1}^{k} P(c_j|x) = 1$

$P(c_r)$ is the class prior probability

and the ANN is trained using the scaled conjugate gradient algorithm, [34] provides an elaborate explanation on this algorithm. The selected loss function for this training is cross-entropy which is given in (2) [33]:

$$E = -\frac{1}{n}\sum_{i=1}^{n}\sum_{j=1}^{k} t_{ij}\ln(y_{ij}) + (1 - t_{ij})\ln(1 - y_{ij}) \quad (2)$$

Where

E is the loss function

N is the number of samples

K is the number of classes

$t_{i,j}$ means the i^{th} sample belongs to the j^{th} class

y_{ij} is ANN response for sample i for class j

As mentioned in section 2.2 sEMG has some random properties and inherited noises associated with it; thus, before feeding the sEMG data to the estimator it needs to undergo a feature extraction process. This process serves two key purposes:

1. Dimension reduction and normalization.
2. Amplify useful data and suppress noises.

Then the classifier will use the extracted features array instead of the sEMG data to do the classification.

We have chosen the following time-domain features:

1. Mean Absolute Value; $MAV = \frac{1}{N}\sum_{n=1}^{N}|x_n|$
2. Number of Zero Crossings; $NZC = \sum_{n=1}^{N-1} s(x_i, x_{i+1})$

   Where $s(x,y) = \begin{cases} 1\ if (x \cdot y) < 0 \\ 0\ if\ (x \cdot y) \ge 0 \end{cases}$
3. Number of Slope Sign Changes; $SSC = \sum_{n=2}^{N-1} ss(Sl_i, Sl_{i+1})$

   Where $ss(x,y) = \begin{cases} 1\ if (x \cdot y) < 0 \\ 0\ if\ (x \cdot y) \ge 0 \end{cases}$ and $Sl_i = \frac{y_i - y_{i-1}}{x_i - x_{i-1}}$
4. Root Mean Square Value; $RMS = \sqrt{\frac{1}{N}\sum_{n=1}^{N} x_n^2}$
5. Variance within each Channel; $ChVar = \frac{1}{N-1}\sum_{n=1}^{N}|x_n - \mu|^2$

   Where $\mu = \frac{1}{N}\sum_{n=1}^{N} x_n$
6. Variance Across Channels; $AChVar = \frac{1}{nCh-1}\sum_{n=1}^{nCh}\left|x_{Ch_n} - \mu\right|^2$

   Where $\mu = \frac{1}{nCh}\sum_{n=1}^{nCh} x_{Ch_n}$
7. RMS Difference between Agonist (Ag) and Antagonist $(Antg)$ Muscles; $RMS_{Diff} = \sum_{n=1}^{N_{Ag}} RMS_n - \sum_{n=1}^{N_{Antg}} RMS_n$
8. Integration of absolute value of sEMG; $I|EMG| = \sum_{n=1}^{N}|x_n| * t_s$

   Where: $t_s = \frac{1}{sF}$; sF is the sampling frequency

9. Signal Power; $SP = \frac{\|x\|^2}{N}$

   Where $\|x\| = \sqrt{x_1^2 + x_2^2 + \cdots + x_N^2}$

10. Average of the Signal RMS Envelope; $RMS_{mean} = \frac{1}{N}\sum_{n=1}^{N} RMS_n$

And the following frequency-domain features:

1. Mean Signal Frequency; $mF = \frac{\sum_{n=1}^{F} SP_n \cdot f_n}{\sum_{n=1}^{F} SP_n}$
2. Average Waveform Length; $W_L = \frac{1}{mF}$

From section 2.3 and the previously mentioned features, we have a 4×12 feature array for each time window. This array has a fixed size regardless of the time window length and therefore helps the classifier to be indifferent to the joint motion speed. Thus, the input layer of the ANN classifier is set to be 48. One positive side effect of having multiple signal features is the compensation for a relatively low number of sEMG signal electrodes [35], as we examined only four muscles in this study.

Since the angular range of motion of a healthy human's elbow joint flexion-extension movement is [0°,145°] [36], we have selected the classes to be 0°, -5°, and +5° to keep the estimation resolution at 5° or 3.45% at a theoretical 100% classification accuracy. Where 0° represents a no-movement, -5° represents 5° flexion movement, and +5° represents 5° extension movement. However, 100% classification accuracy is hard to achieve especially with sEMG data, therefore, we have added two more classes -10°, and +10° to boost the overall classification accuracy. This is true because classes having the same direction but different displacements have more features similarity than classes with the same displacement and different direction. Therefore, the classifier is more likely to miss classify +5° as +10° than to miss classify +5° as -5° and vice versa. So, adding these extra two classes will aid in keeping the classification accuracy within 5°. As a result, the output layer of the ANN classifier is set to be 5, corresponding to 5 distinct classes. We have chosen Matlab R2020a to build the estimator and hence the classifier; Figure 2 shows a block diagram of the designed ANN classifier, Figure 3 shows the data flow throughout the elbow joint motion estimation system.

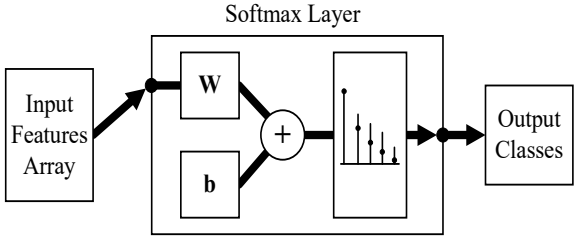

Figure 2: The ANN softmax classifier block diagram.

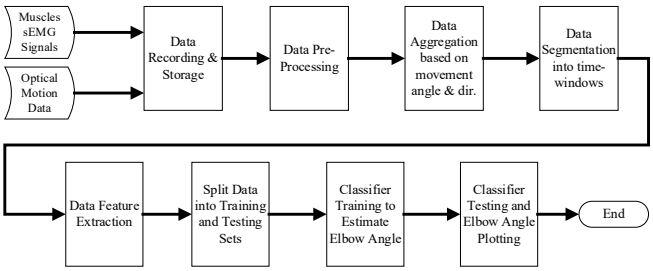

Figure 3: The elbow joint motion estimator flow chart.

2.6. Estimation Results

This section shows the results of the elbow joint movement estimation. We first begin by training the ANN soft-max classifier for the training data set for a maximum of 4000 epochs. Training data and testing data of biceps curl motion confusion matrices are shown in Figure 4 and Figure 5 respectively.

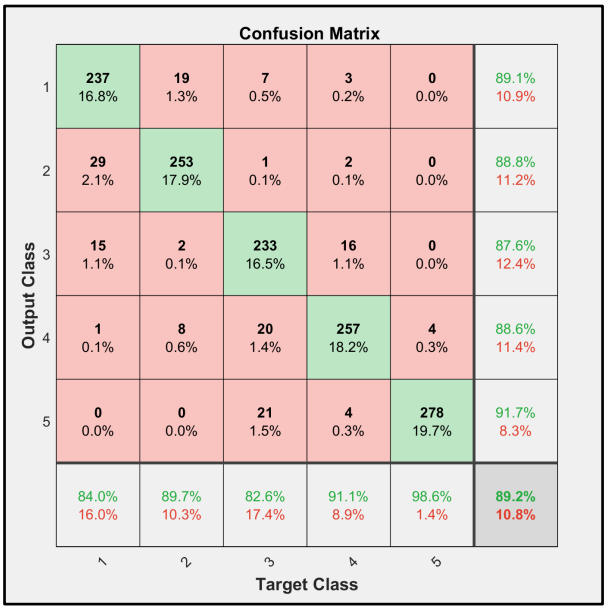

Figure 4: Classifier's confusion matrix for the training data.

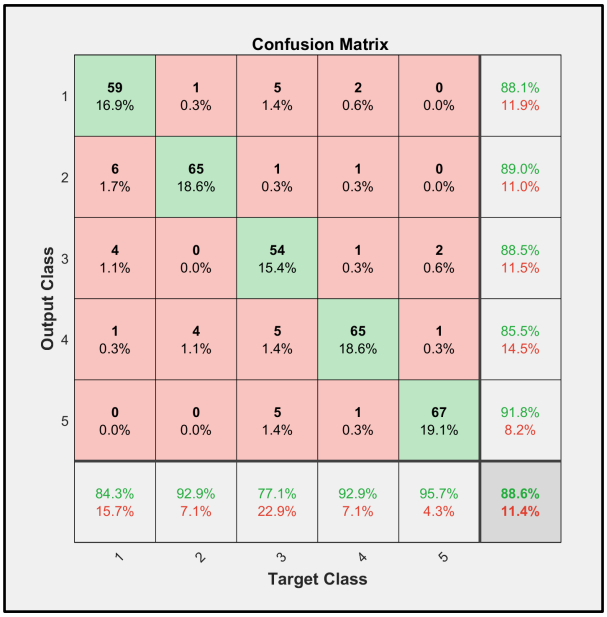

Figure 5: Classifier's confusion matrix for the testing data.

The order of the classes at the output layer of the classifier is as follows +5°, +10°, -5°, -10°, and 0°. If we look closer into Figure 4 and Figure 5 we can notice that most of the confusion happens between the same direction motions. So, if we do a simple probability analysis on the testing data, we can see that adding the two longer displacement classes helps in keeping the error within 5°.

$$k_{+5^\circ} = 88.1\% \; ; k_{+10^\circ} = 89\%$$
$$k_{-5^\circ} = 88.5\% \; ; k_{+10^\circ} = 85.5\%$$
$$k_{+5^\circ or +10^\circ} = 88.1\% + 89\% - (88.1\% \times 89\%) = 98.69\%$$
$$k_{-5^\circ or -10^\circ} = 88.5\% + 85.5\% - (88.5\% + 85.5\%) = 98.33\%$$

Adding two longer displacement classes helps in increasing the accuracy of the classifier in determining the direction to more than 98%. This is true because most of the confusion happens between the same direction movement as they have more similarity across their features.

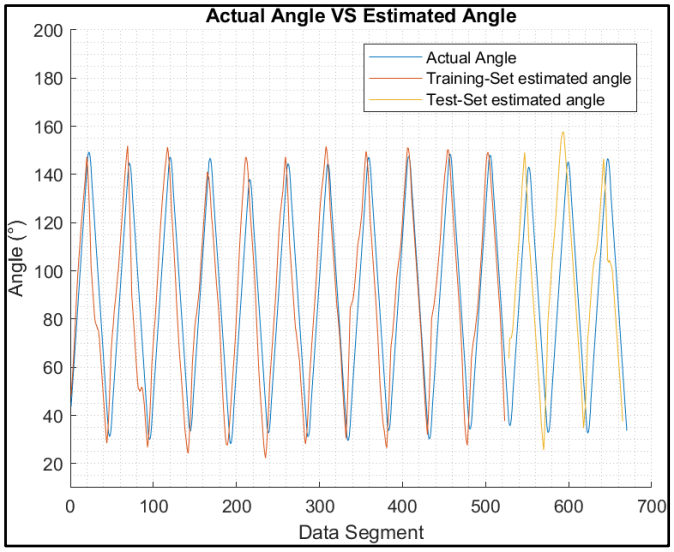

Figure 6: Biceps curls with a 5 pound weight target angle versus estimated angle (confusion for training and testing data are 89.2% and 88.6% respectively).

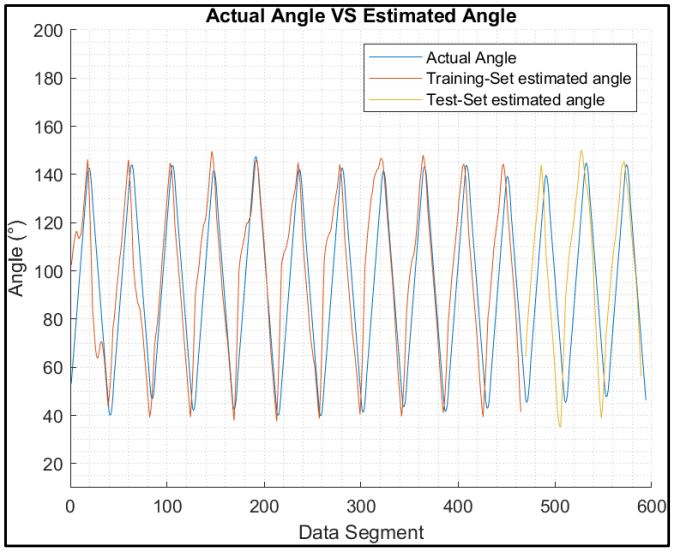

Figure 7: Biceps curls with empty-handed target angle versus estimated angle (confusion for training and testing data are 88.5% and 80% respectively).

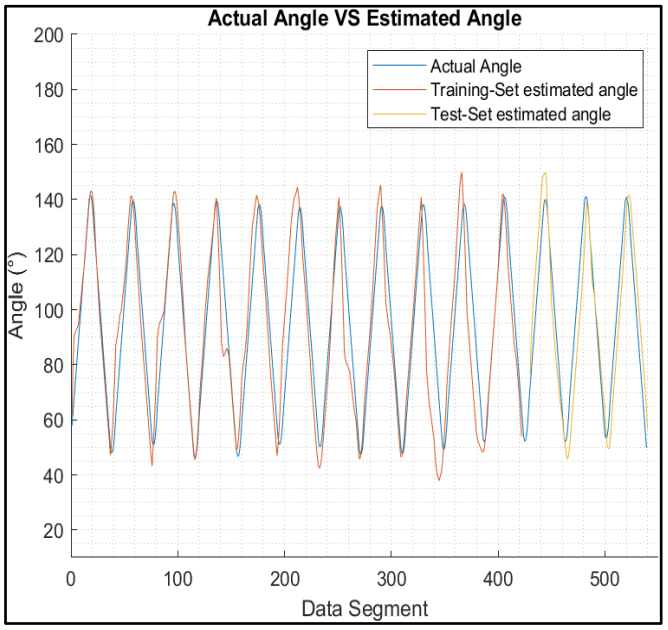

Figure 8: Arm flexion and extension at shoulder level in a horizontal plane target angle versus estimated angle (confusion for training and testing data are 90.4% and 83.5% respectively).

Figure 6, Figure 7, and Figure 8 show the actual joint angle versus estimated angle, training and testing data, for biceps curl with 5 pounds weight, biceps curl empty-handed and arm at shoulder level flexion and extension respectively.

We have chosen Pearson Correlation Coefficient (PCC) as a performance index when comparing the estimated elbow angle against the actual angle because unlike other commonly used performance indices, it is proven to be more accurate in representing the statistical association between two continuous variables as it employs the covariance between the two variables in its calculation [37]. PCC value ranges from +1 to -1, the closest it gets to +1 the more the two vectors are similar to each other. PCC can be found using (9) [16]:

$$PCC(Sig_1, Sig_2) = \frac{cov(Sig_1, Sig_2)}{\sigma_{Sig_1} \cdot \sigma_{Sig_2}} \quad (9)$$

Where

$cov(Sig_1, Sig_2)$ is the covariance of Sig_1 and Sig_2 which is given by (10)

$$cov(A, B) = \frac{1}{N-1} \sum_{i=1}^{N} (A_i - \mu_A)^* (B_i - \mu_B) \quad (10)$$

μ_x is the mean of x, which is given by $\mu_x = \frac{1}{N} \sum_{n=1}^{N} x_n$, and $(*)$ denotes the complex conjugate.

σ_{Sig_1} and σ_{Sig_2} are the standard deviation of Sig_1 and Sig_2 respectively and it's given by (11)

$$S = \sqrt{\frac{1}{N-1} \sum_{n=1}^{N} |A_n - \mu|^2} \quad (11)$$

Table 1 list the PCC values for the estimated elbow joint movements for both training and testing sets for the designated movement.

Table 1: Elbow joint movement estimation correlation coefficient.

Movement	Training / Testing	PCC
Biceps curl with an empty hand	Training	0.92
	Testing	0.92
Biceps curl with 5 lbs.	Training	0.94
	Testing	0.95
Triceps extension with an empty hand	Training	0.92
	Testing	0.91
Triceps extension with 5 lbs.	Training	0.95
	Testing	0.95
Arm flexion at shoulder level in a horizontal plane with an empty hand	Training	0.92
	Testing	0.92
Arm flexion at shoulder level in a horizontal plane with 5 lbs.	Training	0.94
	Testing	0.92

Figure 9 shows the histogram of time-window length in seconds for weighted biceps curls (i.e., 5 lbs) which in turn shows that the estimator was able to work with a variety of time-window sizes for the same angular displacement (and thus variable speeds) and still maintain high accuracy, i.e. +80% in classification and 0.91 in correlation.

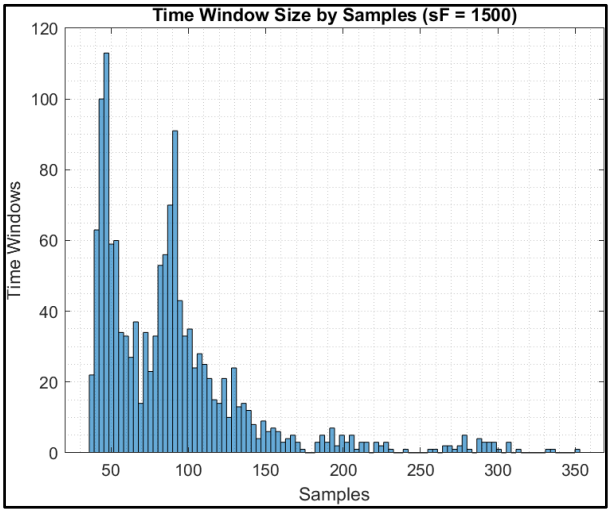

Figure 9: Time-window length in seconds.

3. Discussion

This work describes human's upper limb movement estimation using sEMG data. We have designed an estimator that can estimate elbow joint movement immediately after the neural command sensed through sEMG signals at the muscles. Three muscles were targeted in this work, biceps brachialis, and triceps. The raw sEMG signal underwent preprocessing before it was fed to the estimator. The estimator used a combination of time and frequency domain features extracted for each sEMG channel. The features array is then fed to an ANN-based softmax classifier to be trained to classify five classes in joint angle displacement. The classifier had an accuracy ranging from 80- 90% for different effort levels and limb orientation. The classification was easier for the classifier when the participant carried weight in his hand, which increase the accuracy by 5-7%. The selection of the classes and the accuracy of the classifier translates to PCC between actual and estimated angles ranging from 0.91 to 0.95.

This study aimed to estimate the voluntary movement of upper extremities at the joint level. Since the appendicular skeleton has 126 bones [22], it's not feasible to estimate all the joints movements in one study. To compensate for that we build an estimator that is modular from the software point of view. We believe the developed estimator can work to estimate the movement of any joint in the appendicular skeleton with no modification if we use 4 sEMG channels per joint per degree-of-freedom; assuming that we can properly distinguish agonistic and antagonistic muscles for the chosen joint.

We have chosen the elbow joint for this study because of three main reasons: first, ease of access to its agonistic and antagonistic muscle groups; second, its movement can be done in different planes with respect to the torso; and third, we can vary the joint load easily by asking the participant to hold weights. The last two reasons are essential to check the versatility of the estimator and to make sure it has consistent estimation in different movement conditions. We see this as a necessity because all the related literature reviewed in this study did not account for such variation during joint movement estimation [11–16]. Furthermore, we validate the estimator across the whole dataset by implementing a five-fold cross-validation technique when training and testing the estimator.

Being based on ANN, the softmax classifier took a relatively long time to be trained, and it averaged about 30 minutes for the whole data set. But, on the other hand, the average estimation time per segment was about 1 microsecond, and according to the research in [38], this speed is more than sufficient for real-time applications. We used Windows 10 Pro 64-bit PC with Intel Core i7-4790K CPU and 32 GB RAM and Matlab R2020a to train and test the estimator, which can be a valid option for some but not all Human Machine Interface (HMI) applications targeted to benefit from this study.

The developed estimator can predict the current data segment joint angle with high accuracy regardless of the previous and the next data segment angle estimation accuracy. In other words, misestimation in a single data segment doesn't affect the consecutive data segments. Moreover, due to the selected movement classes, any misestimation will stay within the set 5° resolution which is reflected by the high PCC values shown in Table 1. The choice of features across time-domain and frequency-domain, the choice of classes, and the choice of the classifier all contributed to high estimation accuracy with

0.91 to 0.95 correlation between actual and estimated elbow angle by using only four sEMG sensors on the joint's agonistic and antagonistic muscles.

4. Conclusion

The designed estimator achieved higher accuracy in joint movement estimation regardless of the joint orientation, speed, or effort level than the similar work reviewed in this paper. Which introduces the ability to continuously track the intended movement of the elbow joint with more than 90% correlation. Although the proposed estimator in this work doesn't have 100% joint movement estimation accuracy, section 2.6 and Figures 5 to 8 show that the estimator has over 98% accuracy in predicting the direction of the movement even if it makes a mistake whether the movement is 5° or 10°, as its error margin to predict the wrong direction of movement is less than 2%.

And since the sEMG signals from able-bodied can be used to simulate the human limbs response in amputees [17,39,40], this work can be of great help towards a more natural myoelectric-prosthesis action, and it can also be used to other HMI applications.

References

[1] G. Hefftner, W. Zucchini, G.G. Jaros, "The electromyogram (EMG) as a control signal for functional neuromuscular stimulation. I. Autoregressive modeling as a means of EMG signature discrimination," *IEEE Transactions on Biomedical Engineering*, vol. 35, no. 4, pp. 230–237, 1988, doi:10.1109/10.1370.

[2] G. Hefftner, G.G. Jaros, "The electromyogram (EMG) as a control signal for functional neuromuscular stimulation. II. Practical demonstration of the EMG signature discrimination system," *IEEE Transactions on Biomedical Engineering*, vol. 35, no. 4, pp. 238–242, 1988, doi:10.1109/10.1371.

[3] J. V. Basmajian, C.J. De Luca, Muscle Alives: Their Functions Revealed by Electromyographic, 5th ed, Williams & Wilkins, Baltimore, 1985.

[4] Z. Ju, G. Ouyang, H. Liu, "EMG-EMG correlation analysis for human hand movements," *Proceedings of the 2013 IEEE Workshop on Robotic Intelligence in Informationally Structured Space, RiiSS 2013 - 2013 IEEE Symposium Series on Computational Intelligence, SSCI 2013*, no. Mi, pp. 38–42, 2013, doi:10.1109/RiiSS.2013.6607927.

[5] P.C. Doerschuk, D.E. Gustafson, A.S. Willsky, "Upper Extremity Limb Function Discrimination Using EMG Signal Analysis," *IEEE Transactions on Biomedical Engineering*, vol. BME-30, no. 1, pp. 18–29, 1983, doi:10.1109/TBME.1983.325162.

[6] M. Asghari Oskoei, H. Hu, "Myoelectric control systems-A survey," *Biomedical Signal Processing and Control*, vol. 2, no. 4, pp. 275–294, 2007, doi:10.1016/j.bspc.2007.07.009.

[7] M. Dyson, K. Nazarpour, "Data Driven Spatial Filtering Can Enhance Abstract Myoelectric Control in Amputees," *2018 40th Annual International Conference of the IEEE Engineering in Medicine and Biology Society (EMBC)*, pp. 3770–3773, 2018.

[8] L.A. Johnson, A.J. Fuglevand, "Mimicking muscle activity with electrical stimulation," *Journal of Neural Engineering*, vol. 8, no. 1, pp. 1–25, 2011, doi:10.1088/1741-2560/8/1/016009.

[9] L.H. Smith, L.J. Hargrove, "Comparison of surface and intramuscular EMG pattern recognition for simultaneous wrist/hand motion classification," *Proceedings of the Annual International Conference of the IEEE Engineering in Medicine and Biology Society, EMBS*, pp. 4223–4226, 2013, doi:10.1109/EMBC.2013.6610477.

[10] E.N. Kamavuako, J.C. Rosenvang, R. Horup, W. Jensen, D. Farina, K.B. Englehart, "Surface versus untargeted intramuscular EMG based classification of simultaneous and dynamically changing movements," *IEEE Transactions on Neural Systems and Rehabilitation Engineering*, vol. 21, no. 6, pp. 992–998, 2013, doi:10.1109/TNSRE.2013.2248750.

[11] Y.M. Aung, A. Al-Jumaily, "Estimation of upper limb joint angle using surface EMG signal," *International Journal of Advanced Robotic Systems*, vol. 10, , pp. 1–8, 2013, doi:10.5772/56717.

[12] T. Uchiyama, T. Bessho, K. Akazawa, "Static torque — angle relation of human elbow joint estimated with artificial neural network technique," *Journal of Biomechanics*, vol. 31, , pp. 545–554, 1998.

[13] Triwiyanto, O. Wahyunggoro, H.A. Nugroho, Herianto, "Evaluating the linear regression of Kalman filter model on elbow joint angle estimation using electromyography signal," in *AIP Conference Proceedings*, 020004, 2018, doi:10.1063/1.5054408.

[14] Q.L. Li, Y. Song, Z.G. Hou, "Estimation of Lower Limb Periodic Motions from sEMG Using Least Squares Support Vector Regression," *Neural Processing Letters*, vol. 41, no. 3, pp. 371–388, 2015, doi:10.1007/s11063-014-9391-4.

[15] F. Xiao, Y. Wang, Y. Gao, Y. Zhu, J. Zhao, "Continuous estimation of joint angle from electromyography using multiple time-delayed features and random forests," *Biomedical Signal Processing and Control*, vol. 39, no. December, pp. 303–311, 2018, doi:10.1016/j.bspc.2017.08.015.

[16] F. Xiao, Y. Wang, Y. Gao, Y. Zhu, J. Zhao, "Continuous estimation of elbow joint angle by multiple features of surface electromyographic using grey features weighted support vector machine," *Journal of Medical Imaging and Health Informatics*, vol. 7, no. 3, pp. 574–583, 2017, doi:10.1166/jmihi.2017.2054.

[17] J.G. Ngeo, T. Tamei, T. Shibata, "Continuous and simultaneous estimation of finger kinematics using inputs from an EMG-to-muscle activation model," *Journal of NeuroEngineering and Rehabilitation*, vol. 11, no. 1, pp. 1–14, 2014, doi:10.1186/1743-0003-11-122.

[18] S. Wang, Y. Gao, J. Zhao, T. Yang, Y. Zhu, "Prediction of sEMG-based tremor joint angle using the RBF neural network," *2012 IEEE International Conference on Mechatronics and Automation, ICMA 2012*, pp. 2103–2108, 2012, doi:10.1109/ICMA.2012.6285668.

[19] D. Van Der Riet, R. Stopforth, G. Bright, O. Diegel, "An overview and comparison of upper limb prosthetics," *2013 Africon*, vol. 9, no. 2, pp. 1–8, 2013, doi:10.1109/AFRCON.2013.6757590.

[20] K. Nurhanim, I. Elamvazuthi, P. Vasant, S. Parasuraman, "Determination of Mathematical Model and Torque Estimation of s-EMG Signals based on Genetic Algorithm," vol. 4, no. 5, pp. 135–139, 2013.

[21] D. Shin, J. Kim, Y. Koike, "A Myokinetic Arm Model for Estimating Joint Torque and Stiffness From EMG Signals During Maintained Posture," *Journal of Neurophysiology*, vol. 101, no. 1, pp. 387–401, 2009, doi:10.1152/jn.00584.2007.

[22] R.L. Drake, A.W. Vogl, A.W.M. Mitchell, GRAY'S ANATOMY FOR STUDENTS, THIRD EDIT, CHURCHILL LIVINGSTONE ELSEVIER, Philadelphia, Pa, 2015.

[23] S. Fornalski, R. Gupta, T.Q. Lee, "Anatomy and biomechanics of the elbow joint," *Techniques in Hand & Upper Extremity Surgery*, vol. 7, no. 4, pp. 168–178, 2003, doi:10.1055/s-0033-1361587.

[24] M. Gazzoni, N. Celadon, D. Mastrapasqua, M. Paleari, V. Margaria, P. Ariano, "Quantifying Forearm Muscle Activity during Wrist and Finger Movements by Means of Multi-Channel Electromyography," *PLoS ONE*, vol. 9, no. 10, pp. e109943, 2014, doi:10.1371/journal.pone.0109943.

[25] M.B.I. Reaz, M.S. Hussain, F. Mohd-Yasin, "Techniques of EMG signal analysis: Detection, processing, classification and applications," *Biological Procedures Online*, vol. 8, no. 1, pp. 11–35, 2006, doi:10.1251/bpo115.

[26] Y. Zhang, P. Xu, P. Li, K. Duan, Y. Wen, Q. Yang, T. Zhang, "Noise - assisted multivariate empirical mode decomposition for

multichannel EMG signals," *Biomedical Engineering Online*, vol. 16, no. 1, pp. 1–17, 2017, doi:10.1186/s12938-017-0397-9.
[27] M. Haris, P. Chakraborty, B.V. Rao, "EMG signal based finger movement recognition for prosthetic hand control," *International Conference Communication, Control and Intelligent Systems, CCIS 2015*, pp. 194–198, 2016, doi:10.1109/CCIntelS.2015.7437907.
[28] R.H. Chowdhury, M.B.I. Reaz, M.A. Bin Mohd Ali, A.A.A. Bakar, K. Chellappan, T.G. Chang, "Surface electromyography signal processing and classification techniques," *Sensors (Switzerland)*, vol. 13, no. 9, pp. 12431–12466, 2013, doi:10.3390/s130912431.
[29] S. Muceli, A.T. Boye, A. Avella, D. Farina, "Identifying Representative Synergy Matrices for Describing Muscular Activation Patterns During Multidirectional Reaching in the Horizontal Plane," *Journal of Neurophysiology*, vol. 103, no. 3, pp. 1532–1542, 2010, doi:10.1152.
[30] N. Nazmi, M. Abdul Rahman, S.-I. Yamamoto, S. Ahmad, H. Zamzuri, S. Mazlan, "A Review of Classification Techniques of EMG Signals during Isotonic and Isometric Contractions," *Sensors*, vol. 16, no. 8, pp. 1304, 2016, doi:10.3390/s16081304.
[31] T.A.K. Guanglin Li, Aimee E. Schultz, "Quantifying Pattern Recognition—Based Myoelectric Control of Multifunctional Transradial Prostheses," *IEEE TRANSACTIONS ON NEURAL SYSTEMS AND REHABILITATION ENGINEERING*, vol. 18, no. 2, pp. 185–192, 2010, doi:10.1109/TNSRE.2009.2039619.
[32] E. Scheme, K. Englehart, "Electromyogram pattern recognition for control of powered upper-limb prostheses: State of the art and challenges for clinical use," *Journal of Rehabilitation Research & Development*, vol. 48, no. 6, pp. 643–660, 2011, doi:10.1682/JRRD.2010.09.0177.
[33] C. Bishop, Pattern Recognition and Machine Learning, Springer, 2006.
[34] J.R. Shewchuk, An Introduction to the Conjugate Gradient Method Without the Agonizing Pain, 1994.
[35] N. Miljković, M.S. Isaković, "Effect of the sEMG electrode (re)placement and feature set size on the hand movement recognition," *Biomedical Signal Processing and Control*, vol. 64, , pp. 102292, 2021, doi:10.1016/j.bspc.2020.102292.
[36] C.D. Bryce, A.D. Armstrong, "Anatomy and Biomechanics of the Elbow," *Orthopedic Clinics of North America*, vol. 39, no. 2, pp. 141–154, 2008, doi:10.1016/j.ocl.2007.12.001.
[37] J. Benesty, J. Chen, Y. Huang, "On the importance of the pearson correlation coefficient in noise reduction," *IEEE Transactions on Audio, Speech and Language Processing*, vol. 16, no. 4, pp. 757–765, 2008, doi:10.1109/TASL.2008.919072.
[38] A.J. Young, L.J. Hargrove, T.A. Kuiken, S. Member, "The Effects of Electrode Size and Orientation on the Sensitivity of Myoelectric Pattern Recognition Systems to Electrode Shift," *IEEE Transactions on Biomedical Engineering*, vol. 58, no. 9, pp. 2537–2544, 2011, doi:10.1109/TBME.2011.2159216.
[39] E. Campbell, A. Phinyomark, A.H. Al-timemy, R.N. Khushaba, G. Petri, "Differences in EMG Feature Space between Able-Bodied and Amputee Subjects for Myoelectric Control," *2019 9th International IEEE/EMBS Conference on Neural Engineering (NER)*, pp. 33–36, 2019.
[40] V. Ravindra, C. Castellini, "A comparative analysis of three non-invasive human-machine interfaces for the disabled," *Frontiers in Neurorobotics*, vol. 8, no. October, pp. 1–10, 2014, doi:10.3389/fnbot.2014.00024.

Received: 15 March, 2024, Revised: 10 April, 2024, Accepted: 11 April, 2024, Online: 26 April, 2024

DOI: https://doi.org/10.55708/js0304002

Comprehensive E-learning of Mathematics using the Halomda Platform enhanced with AI tools

Philip Slobodsky[1], Mariana Durcheva*[2,3]

[1]Halomda Educational Software, Rishon LeZion, Israel
[2]Sami Shamoon College of Engineering, Mathematics Department, Ashdod, Israel
[3]TU-Sofia, Informatics Department, Sofia, Bulgaria
*Corresponding author: Mariana Durcheva, Rishon LeZion, Israel, mdurcheva66@gmail.com

ABSTRACT: The method of assessment affects on learning by determining how students manage their time and prioritize subjects. It is widely accepted that students may demonstrate different skills in different assessment formats. The authors demonstrated how e-assessment through the Halomda educational platform can not only improve student learning outcomes, but also enrich their learning experiences. In addition, it is shown how ChatGPT integrated with two new math exploration tools into proprietary Chat-Mat™ module, can help students learn at home and in the classroom, as well as support teachers in their daily work of reviewing student assignments. The outcomes of teaching courses with Halomda not only reveal impressive student performance on final exams but also illustrate a strong correlation between exam scores and weekly assignment grades.

KEYWORDS: E-assessment, E-learning, Halomda educational platform, ChatGPT.

1. Introduction

Like other learning activities, various methods of e-learning are available, tailored to the specific knowledge and skills being achieved. As for the assessment, it is conducted considering the context and purpose, acknowledging that learners may demonstrate varying strengths in different assessment formats and that when students are actively engaged in the activities, it results in deeper thinking and long-term retention of learned concepts [1]. The method of assessment plays a key role in shaping learning outcomes, impacting how students allocate their time and which areas they prioritize to focus on [2-3]. Assessment is typically categorized into the following types: (1) formative assessment, which serves developmental purposes and occurs during the learning process, (2) summative assessment, which aims to evaluate whether students have acquired the expected knowledge or skills, (3) continuous assessment, which means that both formative and summative assignments are used during the course. The feedback provided through formative assessment assists students in tracking their learning progress and serves as a motivational tool.

E-assessment finds broad application, especially in the realms of formative and continuous assessment. Several authors [4] highlighted the fact that e-assessment employs traditional assessment methods but facilitated via online processes and digital tools. However, it could be pointed out that e-learning and e-assessment are not only digital tools, for instance, "many students take e-assessments primarily for the marks, but in doing so, they learn from the questions and especially the feedback" [5]. As digital technology becomes more accessible in education, educators worldwide are increasingly tasked with addressing its potential impact on the academic success of the students. In [6] is argued that when interacting with dialog-based AI models, the goal and context of the desired content should be clearly and concisely defined, and guidance should be provided by adding the necessary instructions and parameters for the appropriate outcome. The authors agree with the authors of [7], that there are two main approaches in technology-assisted assessment, namely - assessment with technology and assessment through technology.

Of course, e-learning and e-assessment has its own challenges. Cheating has become a greater problem with increased use of e-assessment [8-9], since cheating and

plagiarism undermine the validity and reliability of the e-assessment process, eroding students' trust in its integrity [10-12], and, of course, cheating poses a serious threat to important university exams whether they are conducted on campus or online [13]. Students' cheating and plagiarism with regards to e-assessment and using AI technologies are object of research of different authors [14-15], [8], [11]. One approach to mitigate cheating in e-assessment is through the utilization of student authentication and authorship checking systems, like the TeSLA system [8-9], [11], [16]. However, such strategies to combat cheating are particularly well-suited for humanities courses and offer limited effectiveness in engineering disciplines [17]. Hence, biometric and plagiarism-based checking systems represent just a few of the effective measures to mitigate cheating. One potential way to prevent online assessment cheating is to provide each student with unique test instructions, questions, and results. However, creating and administering personalized assessments for each student requires significant preparation time and may not be practical for widespread implementation. To overcome this problem, the use of computer-based assessment tools can help streamline the process and reduce the time required for setup. Various tools are available in widely used learning management systems (LMS) to create tests or multiple-choice assignments, allowing students to submit written assignments to the teacher for manual grading.

Following the increasing usage of AI technologies, and specifically ChatGPT, in education and learning, and exponentially growing number of research in this field, the Halomda developed a unique technology enabling students to create prompts including complex math expressions, to feed them into the built-in ChatGPT, and to use the answers in self-learning. The authors share the hope of the authors of [6] that by overcoming concerns about plagiarism and leveraging the potential of artificial intelligence tools to remove existing barriers to learning, "the educational community will flourish in an increasingly AI-enhanced world".

This paper is organized as follows: Section 2 discusses the related systems in the field of a math e-assessment; Section 3 presents the abilities of the Halomda system; Section 4 is devoted to the e-learning and e-assessment based on the Halomda platform; Section 5 draws conclusions.

2. E-assessment in higher mathematics courses

The use of e-assessment in higher mathematics courses has been shown to be successful in various studies. In [18], the authors stated that the implementation of e-assessment strategies, particularly using multiple-choice questions in Moodle, led to improvements in teaching and learning processes. In [19], the author further supported this, demonstrating the effectiveness of online quizzes as a form of assessment in pure mathematics. However, in [20] is highlighted the need for further research on the practice of assessment in proctored and unproctored math e-learning courses, particularly in relation to academic integrity. Some known systems that support online assignments in mathematics, are: STACK [21], WebAssign [22], WeBWorK [23], Numbas [24]. These systems primarily target basic mathematics, which imposes limitations on the complexity of problems that can be presented.

STACK utilizes a computer algebra system (CAS) called Maxima, which is capable of handling mathematical tasks such as manipulating mathematical expressions. The primary objective of the system is to evaluate students' mathematical responses, generate problems, provide feedback, assign numerical grades, and create internal notes for subsequent analysis. The strength of CAS lies in its capacity to verify algebraic equivalence. However, if it is crucial to differentiate between different forms of answers in a given exercise, the exercise creator must specify in advance which answer formats are acceptable. Once the exercises are created, they can be reused multiple times, thereby reducing the time and workload for teachers. Furthermore, since the system operates independently of teacher supervision, assistants, or classroom availability, students can access it at any time of day or from any location. It's evident that not all question types are suitable for implementation with CAS. Assessing skills such as proof writing and other forms of reasoning cannot yet be automated [25]. Challenges that students may face with STACK often arise from attempts to use unfamiliar syntax when entering answers [26].

WebAssign is a versatile web-based instructional system that offers students additional practice opportunities and provides convenient access to their performance assessments. The software underlying the platform identifies mathematically equivalent expressions in the background. The system offers several benefits, including immediate feedback, the ability for multiple attempts, ease of access, and access to online tutoring [26]. The primary drawbacks include the fact that technical difficulties experienced by some students, reduced interaction with instructors leading to possible neglect of assignments; the need to match the system's format precisely when entering answers, and a less user-friendly experience when asking questions in the tutoring center [26]. From our point of view, the utility of WebAssign is somewhat constrained as it primarily serves homework assignments. Additionally, its integration with specific textbooks means that it must be used in conjunction with the selected textbook, further limiting its applicability.

WeBWorK is an open-source online homework system for math and science courses that enables teachers to

publish problems for students to solve online. Supported courses encompass a range of subjects, including college algebra, discrete mathematics, probability and statistics, single and multivariable calculus, differential equations, linear algebra, and complex analysis. However, it is worth noting that the current engineering content available in the WeBWorK library is limited [27]. Furthermore, the utility of the WeBWorK system is constrained by its primary focus on homework assessment.

Numbas is an online assessment system specifically designed for mathematics subjects and offers several benefits [28]. The system excels at formative assessment and uses client-side grading, although it still requires a server to store grades. Numbas makes it easy to create questions using appropriate mathematical notation, and students can enter symbols that are displayed mathematically. The system supports the creation of complex questions with features such as randomization and automatic scoring and can easily integrate with learning management systems. However, there are limitations in using this system including concerns related to infrastructure, support, the required skills in both teachers and students, as well as time constraints [28].

3. The Halomda Platform

The primary didactic advantage of the Halomda platform over the aforementioned e-systems is its ability to integrate the three main methods of mathematical education - Learn, Train, and Test (Figure 1) ([29] – [31]).

The necessity for a universal, user-friendly, simple yet powerful math platform prompted Halomda Educational Software [29] to develop Math-Xpress, initially introduced in 2001 [30]. Subsequently, additional modules have been integrated into the program, forming a multifunctional Math package with a unified user interface.

Figure 1 [29]: Modes of learning

These interconnected modules rely on proprietary computer algebra (CA) and interactive geometry algorithms, enabling linkage between modules that share common objects. The system comprises five modules:

- XPress-Editor - a formula editor that allows graphical WYSIWYG (What You See Is What You Get) editing of math expressions thus enables compiling of new items by unexperienced in programming people [31].
- XPress-Graph - a graph plotter.
- XPress-Geometry - a 2-D and 3-D geometry explorer.
- XPress-Evaluator.
- XPress-Tutor. For e-assessment purposes, it can be used independently; together with the XPress-Task Editor these modules form a comprehensive platform for e-teaching, e-learning, and e-assessment of mathematics courses.

Over the past few years, thousands of problems have been developed to cover courses in arithmetic, elementary algebra, and geometry for primary and intermediate schools, as well as algebra, trigonometry, and introduction to calculus for high schools. Additionally, courses in Calculus, Linear algebra, Differential equations, Probability, and Statistics have also been addressed. Throughout the course, students receive a comprehensive set of basic problems that thoroughly cover the curriculum. Typically, this set comprises 50 to 150 problems, arranged into 13 weekly assignments for one semester [31].

3.1. Typical student interaction with the platform

Throughout the course, students are provided with a comprehensive set of basic problems that cover the entire curriculum. Typically, this set comprises 50 to 150 problems, arranged into 13 weekly assignments for one semester [31]. In Learn mode, students are presented with a series of problems, each of which includes randomly selected parameters to ensure that different attempts produce different initial sets of parameters. Students have the opportunity to request help, which is provided at three levels: General help, which describes a solution method common to all problems within a particular topic; a List of steps to solve a problem with a description of each step; and the Result of each solution step. In Train mode, students are presented with multiple-choice options for the possible results of each step, facilitating extensive and interactive training. In Test mode, no help is provided, and the student is required to complete a series of tasks that simulate the conditions of a regular test.

Usually, students start with Test mode, attempting to solve problems without assistance. The system allows them to quit the test without penalty but limits the number of attempts for each task. If a student exits a Test mode due to difficulty, he can switch to Learn or Train modes to understand how to solve similar problems. Tasks in the Test mode differ from tasks in the Learn and Train modes only in the values of randomly generated parameters. The Learn and Train modes offer more than just problem solving; they include additional educational resources such as links to external files, websites, videos, etc. to enrich the learning experience.

3.2. Mitigating cheating through the Halomda platform

Adaptability of students' responses significantly reduces the likelihood of cheating. For example, requiring

students to enter their answers manually rather than choosing from multiple answer options greatly reduces the likelihood of dishonesty. Math-Xpress uses two approaches to evaluate student responses in exam mode: using so called "semi-intelligent" multiple choice questions (SI-MCQs) and open-ended (OA) mode. This approach is demonstrated with a problem shown in Figure 2:

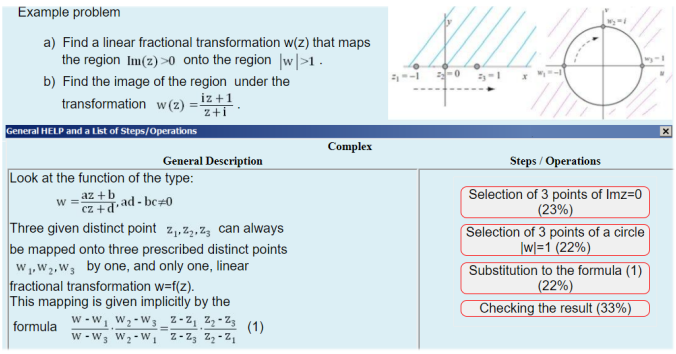

Figure 2 [29]: Task example

During the Learn mode, a student has the possibility to get the results of each step of the problem solution, one of which is the proper answer, and the other three – wrong answers (Figure 3, a). As in usual MCQ-mode, a student can select an answer by clicking on it (in our example: $z_1 = -1, z_2 = i, z_3 = 1$). In case of a wrong answer, a student is provided with short feedback as can be seen in Figure 4.

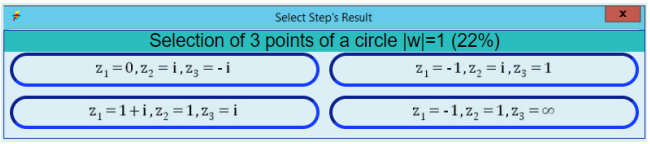

Figure 3 [29]: Step results

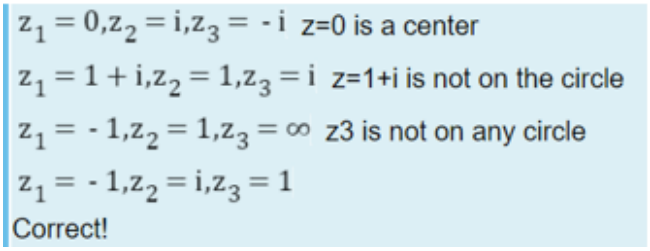

Figure 4 [29]: System comments

Due to the possibility of free-hand typing, the student may decide to enter another expression, for example, just: $(-1;\ i;\ 1)$, and the system will accept them. This ability of the system is provided by the task developer (teacher, instructor), who endeavors to anticipate the most expected options for the correct answer that students can enter.

In open access mode, the result windows are hidden, and students are prompted to manually enter the correct answer. Here, the task designer can choose between two evaluation options: the requirement of strict identity of expressions or their algebraic equivalence. In the first case, the student's answer is compared with all possible answers (both correct and incorrect) given in the task. In the latter case, the comparison is carried out using computer algebra methods to determine algebraic equivalence. For example, the following pairs of expressions are considered equivalent:

$$\frac{2}{\sqrt{2}}, \sqrt{2};\ \ 5^{-2x}, \frac{1}{25^x}\ \ ;\ \ y = 3x + 6, x = \frac{y}{3} - 2$$

An exam may consist of various tasks, each requiring a different assessment method. It is the responsibility of the teacher to determine the most suitable assessment approach for each problem.

The operation of any math assessment system within Moodle (or another Learning Management System (LMS)) can enhance cheating prevention through a combination of random test selection and parameter randomization for tasks. This entails integrating Math core functionalities (such as computer algebra operations, expression evaluation, and test result calculation) into the Moodle code and transferring student data into the Moodle LMS.

Halomda has developed a plugin that enables the system to operate seamlessly within Moodle, facilitating the transfer of results into the Moodle LMS.

3.3. *Integration of ChatGPT into the Chat-Mat™ module of Halomda*

In order to provide students with an easy access to ChatGPT, the last version of Halomda platform includes it as one of a new built-in features: **Graph-Men** (plot and explore graphs) (Figure 5), **Algebraic Calculator** (Equation Solver and Symbolic evaluator in 10 areas of mathematics**)** (Figure 6), **ChatGPT** and recommended **Key Prompts** (Figure 7).

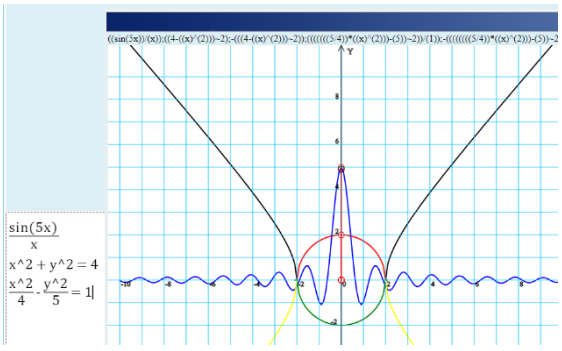

Figure 5: Graph Plotter

In addition to incorporating an AI bot into the system interface, Halomda developed a tool to graphically edit mathematical expressions and present them in the LaTeX format required by ChatGPT. For instance, to compose a prompt for ChatGPT including calculation of the limit: $\lim_{x\to 0} \frac{\sin x}{x}$, it is required to type:

lim_{x\rightarrow0}{(\frac{sinx}{x})}&&

The graphical editor of mathematical expressions offers students the ability to enter limits using the appropriate editor templates (Figure 8), making it easy to include results by copying and pasting into the ChatGPT message box allowing students to easily communicate with the bot. This feature makes communicating with the bot easier, allowing students to interact with it more effectively.

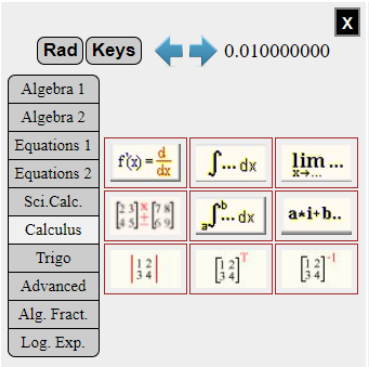

Figure 6: Algebraic Calculator

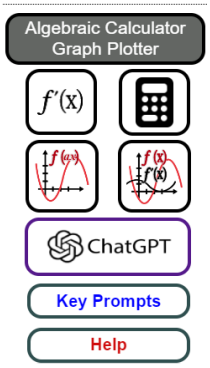

Figure 7: Chat-Mat module

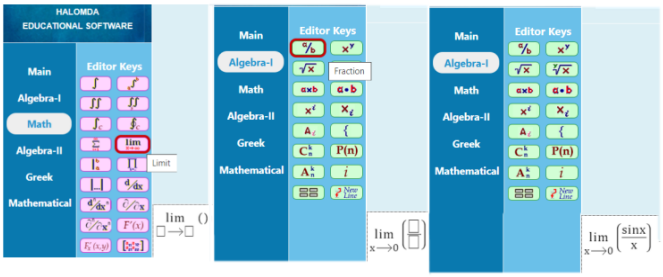

Figure 8: Graphical editing

2 Key Prompts as a new form of self-learning

The main didactical questions arose from most of the publications on using ChatGPT in education of mathematics ([32], [33], [34]) are:

a) How to effectively address the issue of frequently encountering incorrect responses from ChatGPT?

b) In what ways can students utilize ChatGPT as a math tutor beyond just direct problem-solving, considering the occasional inaccuracies?

The suggested answers, based on the teacher's experience and implemented by Halomda in Chat-Math module, can be summarized in the following statement: A student's knowledge of any subject in mathematics is directly proportional to the time spent studying the subject. The more activities offered to students, the greater success is expected!

Following this idea, the authors suggest that the communication with ChatGPT will stimulate the students by presenting other aspects of the problem solving beyond the algebraic technique provided by the Learn and Train modes of the system. To achieve this, the authors recommend that students ask the AI bot diverse questions. These questions (called *prompts*) should enhance their overall knowledge and understanding of the subject and also refine their problem-solving abilities, ultimately leading to greater success in exams. According to [35], "effective prompts are characterized by the following fundamental principles: clarity and precision, contextual information, desired format, and verbosity control, which means that "writing effective prompts is complicated for nontechnical users, requiring creativity, intuition, and iterative refinement".

To help students in composing appropriate prompts, a list of recommended "Key Prompts" is included with each problem in the Learn and Train sections of the system. It consists of 3 types of prompts reflecting the didactical ideas to engage students, including:

1. Solution of the equation; performing algebraic operations; solving integrals; finding derivatives, limits, etc., relevant to the topic.

Although the solution provided by ChatGPT may sometimes be incorrect and/or incomplete, its added value lies in the complementary verbal explanation it offers; the contextual Help recommends the students to verify the answer using the Algebraic Calculator or plot graph with Graph-Man - two other modules included in the Chat-Mat- package.

2. Reminding definitions, theorems, proofs relevant to the subject.

3. Asking broad questions about history, practical applications, "tricky" or amusing questions (like paradoxes, etc.).

Providing students with a list of possible (recommended) prompts not only teaches them to compose their own prompts but also enhances their learning experience by providing additional content required for a deeper comprehension of the subject matter.

The only tool to communicate with ChatGPT is a prompt. In the case where a student is interested in asking for help in solving math problems from class assignments, it is enough to copy the question in the ChatGPT message window, while writing the mathematical expressions in LaTeX format. To achieve this, the Chat-Mat module of the

Halomda platform includes a tool for editing and copying expressions in ChatGPT.

In addition to entering mathematical expressions for evaluation, it is useful to write them so that ChatGPT generates a concise but comprehensive answer. To demonstrate the students how to write math prompts, a short Instructions containing the rules and recommendations are included in the list of Key Prompts, thus completing the didactical need for effective use of ChatCPT.

The role of Key Prompts is two-fold: firstly, to demonstrate students how to formulate math prompts, and secondly, to enhance the overall value of the course, as previously outlined.

The combination of three exploration tools – Key Prompts, Algebraic Calculator and Graph Plotter - allows students to not only observe the solution (provided by ChatGPT), but also check its correctness using the Algebraic Calculator, receive explanations from ChatGPT, and visualize and check it using the Graph Plotter.

The following example demonstrates the use of the Chat-Mat™ module to solve the following:

Problem 1. Find the domain of the function

$$f(x) = 3\log_2(x+4) - 1 + \log_2(x-2)$$

and solve the equation:

$$3\log_2(x+4) = 1 - \log_2(x-2).$$

ChatGPT 3.5 gives a correct answer to the first question, including detailed explanations (Figure 9), but fails to solve the equation, giving the (correct!) comments for the incorrect calculations (Figure 10 and Figure 11), and final wrong answer (Figure 11).

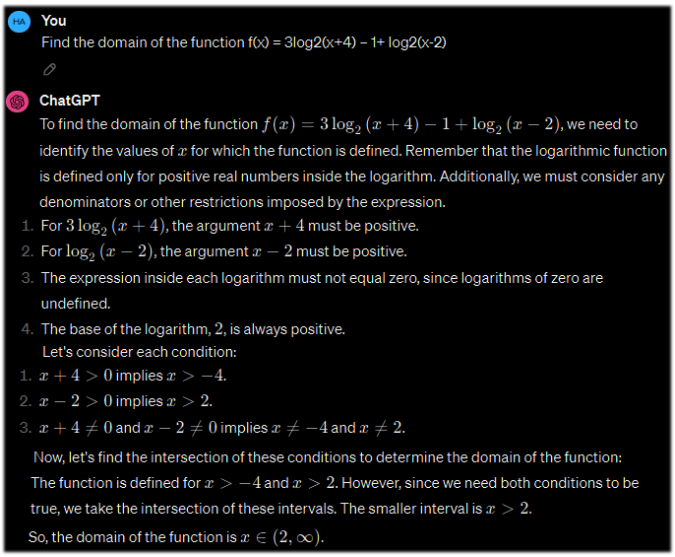

Figure 9: ChatGPT correct answer

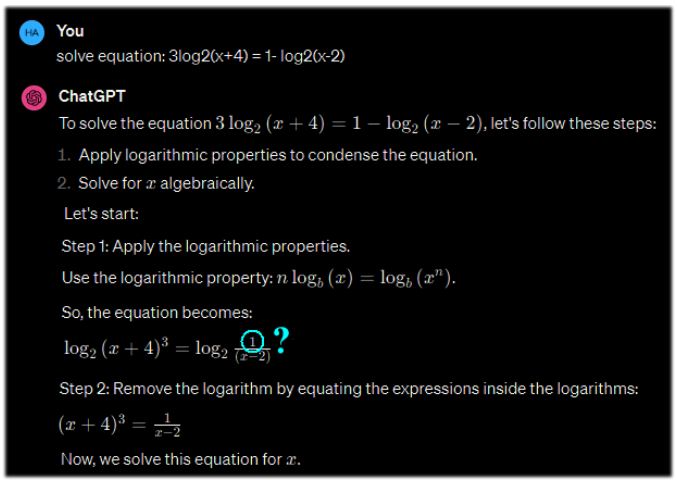

Figure 10: ChatGPT miscalculation

When students are aware of the bot's possible mistakes, they can follow the Instructions and try to check the result in another way, for example, visually - by plotting a corresponding graph using the graph module of Chat-Mat (Figure 12, a), or the Algebraic Calculator (Figure 12, b).

The intersection of the two curves shown in Figure 12,a), representing the graphs of the functions from two sides of the equation, shows that the solution given by the bot is wrong. This may encourage students to analyze the reason why this happened - this is in fact, the (hidden) didactical purpose of the Chat-Mat activity!

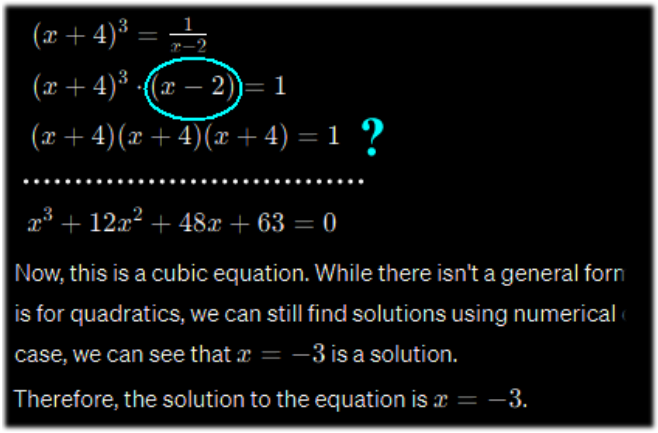

Figure 11: ChatGPT wrong answer

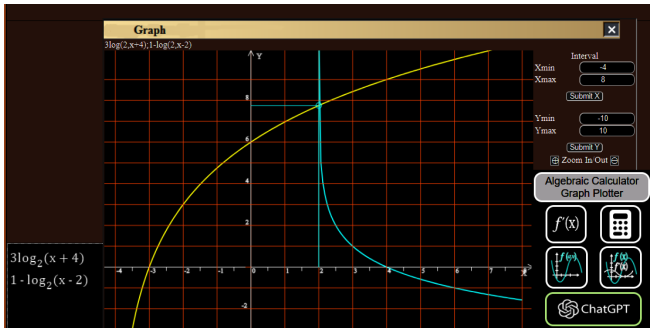

Figure 12 (a): Correct solution by Graph Plotter

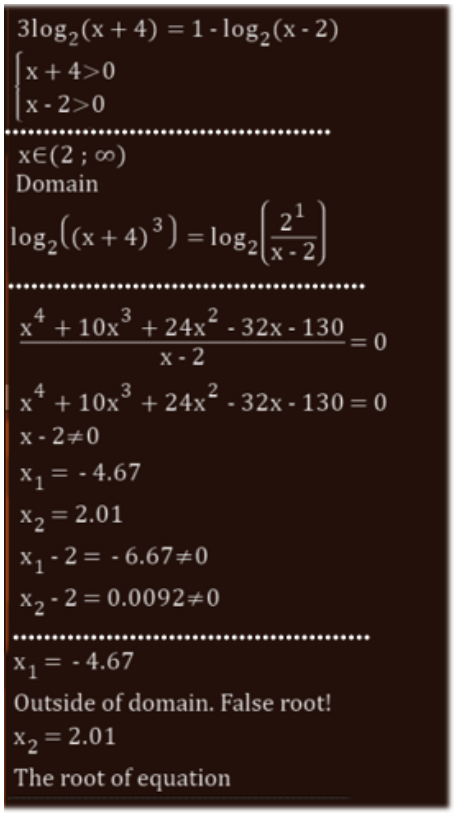

Figure 12 (b): Correct solution by Algebraic Calculator

Students can check each solution step of the bot and discover the mistake in the calculations (Figures 10 and 11), or/and use the Algebraic Calculator (Figure 12, b), compare the solutions and find the mistakes of ChatGPT. The AI abilities of ChatGPT enable them to continue the conversation and try to fix the problem (Figure 13).

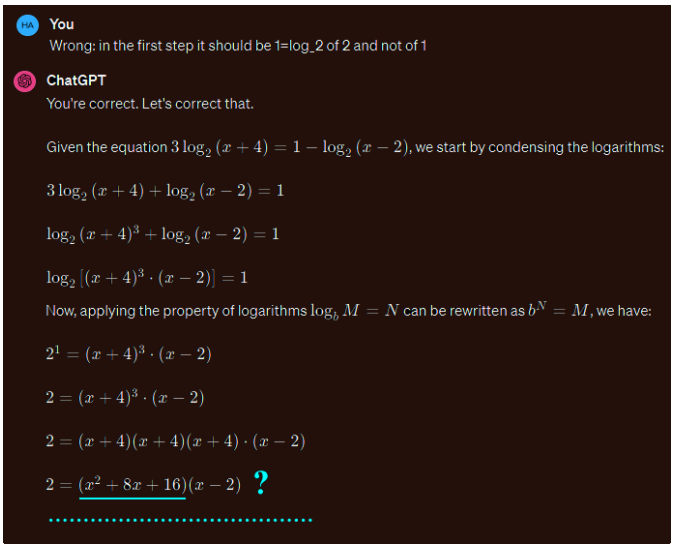

Figure 13: Conversation with ChatGPT

Such interactions between a student and three Chat-Mat tools – ChatGPT, Graph Plotter and Algebraic calculator provide the opportunity for a deeper understanding of the subject, despite the possibility of ChatGPT solving the problem incorrectly.

In order to help students in composing their own prompts, lists of Key Prompts have been created and included into several assignments in Mathematics and Physics, like: Complex Functions, Calculus-I, Transcendental Functions, Basics of Quantum mechanics and more.

4. E-assessment via the Halomda platform

The existence of software for solving mathematical problems has always been problematic due to the possible misuse of it by students during online examination. The Halomda platform does not allow students to get help neither from the built-in Algebraic Calculator or Help option of the system, nor to get access to ChatGPT: all such options are blocked during Test mode (i.e. during the exams).

Using ChatGPT or math-solver software during online exam or even asynchronous test is practically impossible, as long as writing math prompts in LaTeX format necessities using the Halomda's built-in tools (which are typically disabled during Test mode). Additionally, within the Test mode of the Halomda system, solution of a problem often requires answering intermediate steps. Furthermore, the randomization of task parameters helps mitigate cheating, which is crucial for ensuring trusted assessments.

So, the e-assessment offered by the Halomda platform won't interfere with its solving AI abilities.

The benefits of availability of three learning modes: Learn (providing the basic concepts of the subject), Train (allowing practice) and Test (providing opportunities for assessment, including self-assessment) can be summarized as follows:

(1) For students, the platform offers a comprehensive learning tool that includes an interactive e-textbook and extensive training on common problems encountered in the final exam. Combined with the ability to provide instant feedback, the Halomda platform significantly improves the learning process.
(2) For educators, the platform provides an interactive lesson presentation guide along with automatically generated trustworthy grades for midterm assignments.

Over the past decade, five basic Higher Mathematics courses at Ariel University in Israel have employed the Halomda educational platform for teaching and assessment, serving more than 3,000 students annually. The platform's e-assessment module proved indispensable for conducting online assessments during the pandemic [36]. Additionally, Calculus-1 and Elementary Math courses were conducted for 60 students at Talpiot and Orot teachers colleges, respectively. Each course was structured into 13 lessons, either face-to-face or online, followed by problem-solving seminars.

Consequently, students were assigned 13 weekly tasks (mandatory), based on Test mode of the Halomda platform, typically comprising 10 tasks with randomized parameters. Each task included detailed solutions and explanations, functioning as an interactive e-textbook for students and an instructional guide for teachers during online sessions. The Train mode facilitated students' necessary practice, while the Test mode encouraged them to tackle all typical problems, comprehensively covering the course curriculum.

Upon completing the course, students were invited to participate in an online questionnaire. The authors asked about their exam grades as well as the average grade for all Xpress-Tutor assignments. The final exam results revealed both high scores (Figure 14(a)) and a positive correlation between exam grades and weekly assignment grades (Figures 14 a), b)).

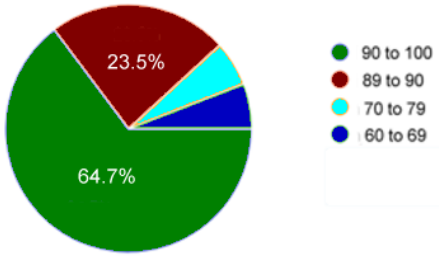

Figure 14 (a): Grades of the final exam [31]

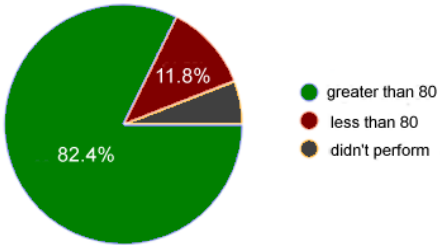

Figure 14 (b): The average grades of assignments [31]

The authors also queried participants about their preferred mode of preparation for the exam. The findings depicted in Figure 15 revealed that Test and Train modes were the most favored options (70.6 and 66.7% respectively).

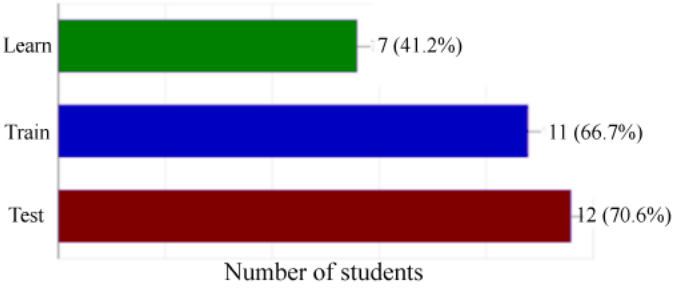

Figure 15: The preferred mode of learning [31]

Figures 16 and 17 display the responses of students to the following queries: To what extent did the system help you in preparing to class exam? (Figure 16) and To what extent was the operation of the system simple and clear? (Figure 17) (on both diagrams the horizontal axes show the rates of correspondent values).

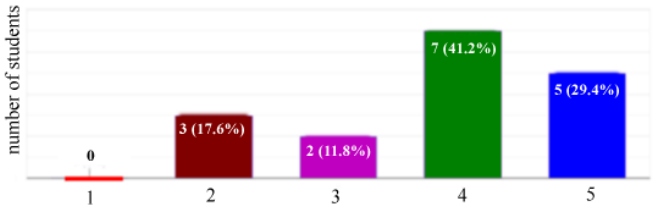

Figure 16: Rate of helpfulness [31]

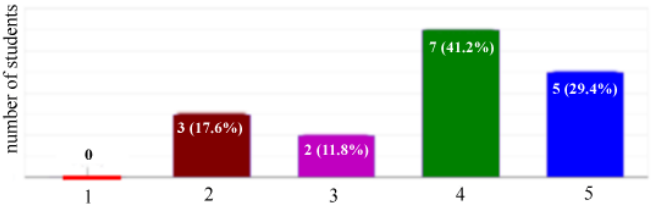

Figure 17: Rating of clarity of the system [31]

The results show that students felt that the system significantly helped them prepare for the exam. They found that the use of the system is simple and clear.

Using the Halomda platform has demonstrated increased student interest and engagement in the subject, as well as significant improvements in learning outcomes.

5. Conclusion

This paper analyzes the most recognized e-learning and e-assessment systems in the field of higher mathematics and highlights the limitations of each of them. Addressing the needs of both students and teachers, Halomda Educational Software has developed Math-Xpress, a versatile, user-friendly and reliable math platform. Math-Xpress offers various modes of interaction with students, including Learn, Train, and Test modes. The integration of the system into LMS-Moodle is a beneficial feature that helps teachers in their routine test checking.

To facilitate the communication of math students with ChatGPT, the latest version of the Halomda platform integrates it as a new built-in feature along with Graph-Men for plotting and exploring graphs, Algebraic Calculator for equation solving and symbolic evaluation, and recommended Key Prompts for various topics across several subjects. The authors believe that dialogue with ChatGPT through properly formulated Prompts can become a new and effective form of self-learning.

Finally, the survey results show a good correlation between final exam scores (which are proctored and administered on campus) and weekly assignment scores. This shows the advantages of using the Halomda platform for e-learning and e-assessment purposes, which can be considered in different directions: the ability of students to

learn from feedback, which significantly enhances students' learning activities (more than 70% of students rated the usefulness of the system as 4 or 5 points), andthe ability to get help from ChatGPT and compare its response with other functions of the Halomda platform.

The further development of the system and the ideas behind it is planned to be focused on the fast growing if AI tools, and particularly their abilities in solving math problems in different areas of mathematics. A study on using of ChatGPT by students of three teachers' colleges has begun and will be presented soon.

References

[1] P.E. Rawlusyk, "Assessment in Higher Education and Student Learning", *Journal of Instructional Pedagogies,* vol. 21, pp. 1-34, 2018. https://bit.ly/2vPtbzT.

[2] J. Biggs, C. Tang, Teaching for Quality Learning at University: What the student does, (3rd ed*).* Maidenhead: McGraw-Hill, 2007.

[3] G. Brown, J. Bull, M. Pendlebury, Assessing student learning in higher education, London: Routledge, 1997.

[4] R. De Villiers, J. Scott-Kennel, R. Larke, "Principles of effective e-assessment: A proposed framework", *Journal of International Business Education*, vol. 11, pp. 65–92, 2016.

[5] M. Greenhow, "Embedding e-assessment in an effective way", *MSOR Connections,* vol. 17, no. 3, – journals.gre.ac.uk., 2019.

[6] B. Eager, R. Brunton, "Prompting Higher Education Towards AI-Augmented Teaching and Learning Practice", *Journal of University Teaching & Learning Practice*, vol. 20, no. 5, 2023, https://doi.org/10.53761/ 1.20.5.02.

[7] P. Drijvers, "Digital assessment of mathematics: Opportunities, issues and criteria", *Mesure et évaluation en éducation*, vol. 41, no. 1, 41-66, 2018, https://doi.org/10.7202/1055896ar.

[8] H. Mellar et al.," Addressing cheating in e-assessment using student authentication and authorship checking systems: teachers' perspectives," *Int. Journal for Educational Integrity,* vol. 14, no. 2, 2018. DOI 10.1007/s40979-018-0025-x.

[9] R. Peytcheva-Forsyth, L. Aleksieva, B. Yovkova, "The Impact of Technology on Cheating and Plagiarism in the Assessment – the teachers' and students' perspectives", *AIP Conference Proceedings* 2048, 020037, 2018, https://doi.org/10.1063/1.5082055.

[10] J. Dermo, "E-assessment and the student learning experience: A survey of student perceptions of e-assessment", *British Journal of Educational Technology*, vol. 40, no. 2, pp. 203–214, 2009, https://doi.org/10.1111/j.1467-8535.2008.00915.x.

[11] S. Kocdar, A. Karadeniz, R. Peytcheva-Forsyth, and V. Stoeva, "Cheating and Plagiarism in E-Assessment: Students' Perspectives", *Open Praxis*, vol. 10 issue 3, July–September 2018, pp. 221–235 (ISSN 2304-070X).

[12] M. E. Rodríguez, A.-E. Guerrero-Roldán, D. Baneres, I. Noguera, "Students' Perceptions of and Behaviors Toward Cheating in Online Education", *IEEE Revista Iberoamericana De Tecnologias Del Aprendizaje*, vol. 16, no. 2, May 2021. Doi: 10.1109/RITA.2021.3089925.

[13] A. Vegendla, G. Sindre, "Mitigation of Cheating in Online Exams: Strengths and Limitations of Biometric Authentication", *Biometric Authentication in Online Learning Environments*, 2019, DOI: 10.4018/978-1-5225-7724-9.ch003.

[14] J. M. Bartley, Assessment is as Assessment does: A conceptual framework for understanding online assessment and measurement, Online assessment and measurement: Foundations and challenges, pp. 1–45, 2005, IGI Global.

[15] S. Stacey, "Cheating on your college essay with ChatGPT", *Business Insider*, https://www.businessinsider. com/professors-say-chatgpt-wont-kill-college-essays-make-education-fairer 2022-12.

[16] M. Ivanova, S. Bhattacharjee, S. Marcel, A. Rozeva, M. Durcheva, "Enhancing Trust in eAssessment - the TeSLA System Solution", *21st Conf. on e-assessment (TEA2018),*10-11 Dec 2018, Amsterdam, The Netherlands, Conf. Proc., https://www.teaconference.org/. arXiv:1905.04985.

[17] M. Durcheva et al., "Innovations in teaching and assessment of engineering courses, supported by authentication and authorship analysis system", *The 45th conference AMEE'19, AIP Conf. Proc.* 2172, 040004 (2019); https://doi.org/10.1063/1.5133514.

[18] J. M. Azevedo, E.P. Oliveira, P.D. Beites, "How Do Mathematics Teachers in Higher Education Look at E-assessment with Multiple-Choice Questions", *International Conference on Computer Supported Education*, 2017, DOI:10.21913/IJEI.V3I2.165.

[19] S. Zegowitz, "Evaluating the use of e-assessment in a first-year pure mathematics module", *Preprint*, 2022, https://arxiv.org/pdf/1908.01028.pdf.

[20] S. Trenholm, "An investigation of assessment in fully asynchronous online math courses", *The International Journal for Educational Integrity, 3*', 2007, DOI:10.21913/IJEI.V3I2.165.

[21] STACK, https://stack-assessment.org.

[22] WebAssign, https://webassign.com.

[23] WeBWorK, https://webwork.maa.org.

[24] Numbas. https://www.numbas.org.uk.

[25] C. J. Sangwin, Computer Aided Assessment of Mathematics. Oxford: Oxford University Press, 2013.

[26] D. Serhan and F. Almeqdadi, "Students' perceptions of using MyMathLab and WebAssign in mathematics classroom", *International Journal of Technology in Education and Science* (IJTES), vol. 4, no.1, pp. 12-17, 2020.

[27] A. G. d'Entremont, P. J. Walls, P. A. Cripton, "Student Feedback and Problem Development for WeBWorK in a Second-Year Mechanical Engineering Program". *Proc. 2017 Canadian Engineering Education Association (CEEA17) Conf.*

[28] V. Challis, R. Cook, and P. Anand, "Priming Numbas for formative assessment in a first-year mathematics unit", In Gregory, S., Warburton, S. & Schier, M. (Eds.), *Back to the Future – ASCILITE '21. Proc. ASCILITE 2021 in Armidale* (pp. 313–318), (2021), https://doi.org/10.14742/ascilite2021.0145.

[29] Halomda. https://halomda.org.

[30] S. Kornstein, "Xpress Formula Editor and Symbolic Calculator", *Mathematics Teacher*, vol. 94, no. 5, May 2001.

[31] P. Slobodsky, M. Durcheva, "E-assessment of Mathematics Courses using the Halomda Platform", *AIP Conf. Proc.* 2939, 050011, 2023, https://doi.org/10.1063/5.0178514.

[32] Y. Wardat, M. Tashtoush, R. AlAli, A. Jarrah, "ChatGPT: A revolutionary tool for teaching and learning mathematics", *Eurasia Journal of Mathematics, Science and Technology Education,* vol. 19, no. 7, em2286, 2023, https://doi.org/10.29333/ejmste/13272.

[33] S. Zhao, Y. Shen, Z. Qi, "Research on ChatGPT-Driven Advanced Mathematics Course", *Academic Journal of Mathematical Sciences,* vol. 4, no. 5, 2023, doi: 10.25236/AJMS.2023.040506.

[34] Rane, Nitin, "Enhancing Mathematical Capabilities through ChatGPT and Similar Generative Artificial Intelligence: Roles and Challenges in Solving Mathematical Problems", 2023, http://dx.doi.org/10.2139/ssrn.4603237.

[35] J. Velásquez-Henao, C.J. Franco-Cardona, L. Cadavid-Higuita, "Prompt Engineering: a methodology for optimizing interactions with AI-Language Models in the field of engineering", *DYNA*, 90 (230), *Especial Conmemoración 90 años*, pp. 9-17, Nov 2023, ISSN 0012-7353, DOI: https://doi.org/10.15446/dyna.v90n230.111700.

[36] P. Slobodsky, A. Shtarkman, A. Kouropatov, "The implementation of e-training and e-assessment system Math-Xpres in development and practical use of system Math-Xpres in development and practical use of math courses at teachers' colleges in Israel during the Corona times", (Unpublished communication), 2022.

JENRS

Received: 30 March, 2024, Revised: 14 April, 2024, Accepted: 15 April, 2024, Online: 30 April, 2024

DOI: https://doi.org/10.55708/js0304003

Numerical Analysis of Riverbank Slope Stability Considering Rainfall, Vegetation and Water Level Fluctuation

Md Tanvir Ahsan, Ji-Peng Wang, Abdelali Dadda*

School of Civil Engineering, Shandong University, Jingshi Road 17922, Jinan 250061, China

*Corresponding author: Abdelali Dadda, Email: abdelali.dadda@sdu.edu.cn

ABSTRACT: The occurrence of landslides and slope instability along riparian zones has been a recurrent phenomenon of substantial concern globally. This paper presents a comprehensive investigation of riverbank slope stability utilizing soils from the Yellow River in China, with a particular emphasis on the effects of water level fluctuations, precipitation, and vegetation. The research examines the interplay of multiple factors influencing slope stability by integrating empirical data from laboratory testing with numerical analysis using Plaxis3D. Salient findings indicate that vegetation significantly enhances riverbank slope stabilization, especially during precipitation events, and that water level fluctuations profoundly impact the mechanical behavior and integrity of riverbank slopes, particularly during rapid drawdown stages. The study underscores the significance of these aspects in riverbank protection and infrastructure development. Despite the rigorous methodology employed, the work acknowledges limitations in numerical modeling and laboratory test scale, highlighting the necessity for more advanced research in geotechnical engineering.

KEYWORDS: Slope stability, Rainfall & Vegetation, Rapid drawdown, Plaxis3D

1. Introduction

Slope stability is a widespread and essential topic in engineering fields. Landslides and debris flows caused by slope instability often result in significant socioeconomic consequences and a significant loss of life [1]. The stability of riverbank slopes is crucial for maintaining the natural balance of riverine ecosystems and protecting human infrastructure located near streams and rivers. The gradual wearing away of riverbanks in multiple locations has a growing influence on the livelihoods of those who live near these sites. The stability of a slope can be influenced by factors such as the shape of the embankment, changes in water levels, and the properties of the soil [2]. The influencing factors of slope instability mainly include internal factors and external (induced) factors. Among them, internal factors can be summarized as geological factors, slope rock and soil properties, slope shape, groundwater, etc.; external factors mainly include climatic conditions (rainfall, temperature), earthquakes, human activities, etc. [3–5]. Regarding the influence of slope stability, various factors do not act independently, but are interrelated, promote each other, and can even transform into each other under certain conditions.

The stability of riverbank slopes in China, particularly along the Yellow and Yangtze Rivers, is profoundly influenced by precipitation and water level drawdown. Research has indicated that these conditions can precipitate landslides, especially in the Three Gorges Reservoir region [6]. Reservoir levels and precipitation have a significant impact on landslide stability, with fluctuations in reservoir levels being the primary influencing factor [7]. The reactivation of significant landslides caused by changes in reservoir levels has been documented, such as the Dasha landslide [8]. An analysis has been conducted on the weakening of soil sliding zones in accumulation landslides produced by rainfall infiltration, emphasizing the gradual development of failure in such scenarios [9].

Precipitation is a primary driver of slope instability [10], impacting riverbank stability through erosion, pore water pressure changes, and soil saturation [11]. Intense or prolonged rainfall events can trigger landslides and slope failures, compromising the structural integrity of

riverbanks [12]. The temporal and spatial distribution of precipitation, as well as antecedent soil moisture conditions, significantly affect the susceptibility of riverbanks to instability. Analyzing the rainfall patterns and their correlation with slope failures is crucial for developing predictive models and early warning systems [13].

A range of physical model experiments have been conducted to investigate the failure mechanisms of soil slopes. Rawat [14] studied the behavior of nailed soil slopes under surcharge loading, finding that the inclination of the nails significantly influenced the load carrying capacity. In [15], the authors conducted centrifuge model tests to analyze the deformation and failure processes of soil slopes, introducing the concept of a shear zone to describe the failure process. The research in [16], showed the importance of considering the stability of unsaturated soil slopes under random rainfall patterns. Since field tests are usually expensive and take a long time, some scholars use indoor model tests to study landslides. Among them, some scholars conducted centrifuge model tests through self-developed centrifuge airborne rainfall simulation devices to study slope stability under rainfall conditions. In [15], the researchers further explored the mechanisms of gradual riverbank collapses, emphasizing the role of seepage exit gradient and the development of partial infiltration failures. A systematic review by [17], identified various control practices for soil erosion in Asian agricultural land, including those related to rainfall and soil slope. In [18], the authors conducted a study on slopes with and without vertical joints. Three types of indoor physical model tests were conducted to study the effects of different rainfall patterns and different slope structures on the deformation and failure process. In [19], the authors took the Pengshan landslide in Zhejiang Province as a prototype and obtained the influence of rainfall intensity and weak interlayer thickness on slope stability based on experimental monitoring data such as pore pressure, earth pressure and slope deformation.

Vegetation plays a dual role in riverbank stability. On one hand, plant roots contribute to slope stabilization by binding soil particles and enhancing cohesion [20]. On the other hand, vegetation can influence slope stability negatively if it impedes water drainage or introduces additional loads during extreme weather events. The type, density, and health of vegetation are critical factors in understanding their impact on riverbank stability [21]. Incorporating vegetation dynamics into stability models is essential for accurate assessments of the overall stability conditions. Various studies have examined the influence of vegetation on the stability of soil slopes. In [22] and [23], the authors both highlight the dual role of vegetation in influencing slope stability, through changes in soil moisture and root reinforcement. In [24] and [25], the authors further emphasize the mechanical and hydrological effects of vegetation, with Cecconi [24] specifically focusing on the positive mechanical effect of deep-rooted grass plants. In [26], the authors highlighted vegetation enhances rainfall infiltration and decreases runoff, reducing slope stability and surficial erosion. Plant transpiration induces higher suctions and hence slope stability. The effect of vegetation in creating dryer soil conditions is more significant than the orientation effect. These studies collectively underscore the significant potential of vegetation in stabilizing soil slopes, and the need for further research to develop reliable field data and models to support this.

Several studies have examined the stability of riverbank slopes using numerical analysis. In[27] and [2], the authors employed finite element methods to evaluate the influence of water level fluctuations and soil characteristics on slope stability. Zaw's research concentrated on rapid drawdown, whereas Haque's study encompassed different embankment conditions. In a study on a riverbank in Malaysia, GeoStudio was employed to model the riverbank based on borehole log reports and other data. The findings highlight that drawdown events significantly impact slope riverbank stability, as evidenced by the fluctuating Factor of Safety values during and after these events [28]. A new contact element model is introduced to simulate the contact friction state on the slide surface, which led to a more accurate analysis of slope stability [29]. Li furthered this work by examining the influence factors, failure modes, and dynamic stability of layered rock slopes under seismic action [30].

A number of studies have utilized both Limit Equilibrium Method (LEM) and Finite Element Method (FEM) in analyzing slope stability. In [31], the authors discovered that the Limit Equilibrium Method (LEM) typically provides a greater factor of safety compared to the Finite Element Method (FEM). Both approaches exhibit a reduction in factor of safety as water level rises. In [32], the researchers pointed out the constraints of LEM and FEM for examining slopes containing clay-rock combinations, recommending the utilization of the discrete element approach as an alternative. In [33], the authors observed that FEM yielded higher factor of safety values compared to other approaches, however both methods showed identical critical slip surface shapes and locations. In [34], the authors suggested a technique that integrates Finite Element Method (FEM) with Limit Equilibrium Method (LEM) to account for the impact of slope deformation on stability. Recent years have witnessed notable progress in the field of slope stability in civil engineering, especially in the enhancement of analysis methods. In [35], the authors discusses the development of deterministic and probabilistic methods, whereas In [36], the authors contrasts the classical limit equilibrium method with the finite element method.

Understanding the complex interactions among the aforementioned factors is essential for effective riverbank management, environmental conservation, and risk mitigation. Studying methods to manage riverbank erosion is crucial for establishing priorities for erosion control and enhancing livelihood resilience. It is imperative to comprehend erosion management techniques and apply them in marginalized regions to aid riverine communities in combating riverbank erosion [37, 38].

This study focuses on the geotechnical aspects of slope stability, specifically targeting the alluvial silt slopes of the Yellow River. It encompasses an experimental setup and data collection, numerical modeling, and a comprehensive analysis of findings. The research is intended to contribute to the broader field of geotechnical engineering, specifically in the context of riverbank erosion and environmental conservation. This research aims to analyze riverbank slope stability by examining the impact of rainfall, vegetation, and water level fluctuations which in this case rapid drawdown. By using empirical data from laboratory experiments. This research seeks to use Plaxis3D for numerical analysis to connect theoretical models and empirical observations, in order to gain a thorough understanding of riverbank dynamics.

- This research will use laboratory experiments to quantitatively study the impact of rainfall on bare and vegetated soil slopes. The investigation includes replicating rainfall conditions and assessing their effect on soil slope. Using this empirical approach will improve the dependability of the numerical models created in Plaxis3D, resulting in a more precise forecast of slope performance in various rainfall conditions.
- The research also critically examines the impact of vegetation on slope stability. Laboratory tests will be conducted to analyze the impact of plants on soil strength and erosion resistance. The data obtained from the experiment will offer vital insights into the relationship between plant roots and soil under different environmental circumstances. This mission seeks to explore the strategic utilization of vegetation to strengthen riverbank slopes.
- Variations in water levels such as rapid drawdown in this case can greatly affect the mechanical characteristics of riverbank soils. The project aims to forecast the influence of variations on slope stability using Plaxis3D, providing valuable insights for riverbank management and infrastructure building near water bodies.
- Thorough integration of numerical and empirical data, the main objective of this research is to combine numerical modeling with empirical data. The project will provide a more detailed knowledge of the elements affecting riverbank stability by integrating the results of Plaxis3D simulations with laboratory observations. This comprehensive method will help create more precise and dependable predictive models.

2. Methodology

2.1. Laboratory Test

2.1.1. Slope model design

The Yellow River alluvial silt slope model was designed based on comprehensive experimental research purposes, research objects, model production operability and the layout of various monitoring devices. The design size of the slope model is 3m × 1.5m × 1.2m (length × width × height), the slope top platform is 1m long, and the slope ratio is 1:1. For vegetated slope the same dimensions has been used.

Figure 1: slope diagram and lab model

2.1.2. Rainfall Simulation System

The NLJY-10 artificial simulated rainfall system, used in the experiment, consists of several components: a rainfall rack measuring 4.0m x 3.0m x 3.2m (length × width × height), a 1000L water tank with a control valve and inlet pipe, a self-priming pump with a 5.5m³/h flow rate, a 20m head, 2214r/min rotation speed, and 0.75KW power, and a network of water pipes. The system's control center is fully automated, displaying rain intensity, operation status, pressure, countdown, and integrating all power control functions. It operates in DCS mode and can create rain pattern project files for automatic control of varying rain intensities over time. The system's rain intensity can be adjusted with a precision of 5%, and it can simulate rain intensities ranging from 5mm/h to 240mm/h. For this research 30mm/h rainfall is used.

Figure 2: Artificial simulated rainfall system

2.1.3. Monitoring System

The experimental setup for monitoring soil and slope stability includes various sensors and a data collector. TDR-315N Soil Volumetric Moisture Sensor to measures

soil moisture content. TEROS-21 for continuously monitoring soil water potential in real-time. SPWP50 Pore Water Pressure Sensor to measures soil pore water pressure. SPS-BOX Soil Pressure Sensor, it measures earth pressure within a specified range and is capable of operating in saturated water conditions. CR350 Data Collector, A low-power device used for measuring sensors, analyzing, and storing data. A laser scanner is used to get the deformation map. Additionally, a camera with automatic continuous shooting is set to capture images every 8 seconds, providing real-time monitoring of slope deformation and damage during rainfall. This comprehensive setup allows for detailed observation and analysis of soil behavior and achieve real-time monitoring and recording of slope deformation and damage during rainfall.

2.1.4. *Test preparation and process*

Preparing and evaluating a slope model in soil engineering requires following a series of essential processes:

- Soil Sample Preparation: The soil is sieved to eliminate impurities and combined with water beyond the ideal moisture level to compensate for evaporation. The soil is uniformly soaked, mixed, packaged, and sealed for 48 hours to guarantee consistent moisture distribution.
- Slope Model Filling: The slope is built with 12 layers, each 10cm deep, employing a method of compacting layers to reach a density of 95%. Particular attention is given to limits, corners, and the installation of monitoring sensors. Following compaction, the slope is manually trimmed to a 1:1 slope ratio and then covered with plastic sheeting for 3 days to allow for moisture equalization.
- Test Process: Before testing, all 35 sensors and data collectors are checked for proper functioning. Cameras and lights are adjusted for optimal visibility, and the rainfall control system is set up. The test involves simulating 30mm/h rainfall until the slope becomes unstable and collapses, closely monitoring the process throughout.

2.2. *Finite element modeling*

Plaxis is a program that utilizes the finite element method to conduct numerical computations for geotechnical issues such as deformation, consolidation, stability, and flow studies. Plaxis allows users to simulate excavations, create structures, and apply loading and unloading to the soil in various phases, mirroring real-world projects [39]. The characteristics in Plaxis facilitate a well-suited modeling procedure. The laboratory model findings are being compared with the results obtained by PLAXIS3D. This process involves dividing the soil into smaller parts for analysis. The equilibrium equations can be solved from the nodes of the elements [40]. At each time step, the equations for individual smaller elements are solved and then combined to estimate the solution for the overall complex model. PLAXIS is a popular Finite Element Method (FEM) tool used for analyzing soils and groundwater movement [41]. It is known for being easy to use while also being able to simulate many real-world aspects. The research utilizes Plaxis3D for several purposes such as initial stress generation, plastic calculations, fully coupled flow-deformation analysis, and safety calculations. PLAXIS can perform a flow-deformation analysis to address the interaction between deformations, consolidation, and groundwater flow simultaneously in a single phase. The software is utilized to simulate the overall stability of the slope model. The objective is to assess the observation during the laboratory slope model test.

2.2.1. *Geometry and mesh*

Following the completion of the slope model test, we have now transitioned into a critical phase where the acquired data is being applied for numerical modeling using Plaxis 3D. To provide a detailed perspective, the physical slope model, which served as the source of experiment data, was used for designing with precise dimensions. The overall structure measured 3 meters in length, 1.5 meters in width, and 1.2 meters in height. The slope top platform is 1m long. Another critical aspect of the model was its slope ratio, which was set at a 1:1 gradient. This ratio, indicating a 45-degree angle, was selected to study the slope stability under a relatively steep condition. The initial slope model in Plaxis is showed in the following figure,

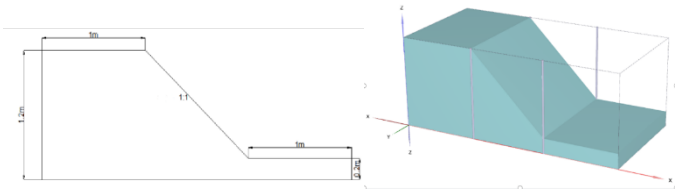

Figure 3: Slope model diagram

Mesh creation occurs next in Plaxis when the modeling phase is finished and the input parameters are set. In Plaxis, the term "mesh" refers to the process of breaking down the modeled soil and structure into smaller, finite components to create a structure that resembles a grid. The finite element analysis is built upon this mesh. More processing power and time are needed for more detailed results. The graphic displays the created mesh is shown in figure 4.

2.2.2. *Parameters*

The Mohr-Coulomb material model is used for the soil and also the Van Genuchten function was used in Plaxis

finite element analysis software to investigate soil behavior and water retention properties. The characteristics are obtained from the laboratory analysis of the Yellow River alluvial silt. The precise values for these parameters were entered into Plaxis and are outlined in the table 1. This method guarantees that the soil analysis is accurate and feasible.

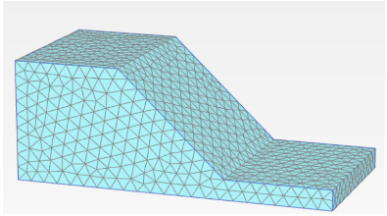

Figure 4: Mesh for the slope model

Table 1: Input parameters for the silty fine sand

Silty Fine Sand		
Property	**Value**	**Unit**
Saturated Unit Weight, γ_{sat}	20.51	KN/m^3
Dry unit weight, γ_d	16.58	KN/m^3
Void ratio	0.649	
Porosity	39.388	%
Cohesion	4.5	KPa
Friction angle	34.7	
Permeability	2.34144	m/day
Poisson's ratio	0.3	
Young's Modulus	32500	KN/m^2
Rainfall	30	mm/h
Saturation	25	%
Node tensile strength	29.72	MPa

2.2.3. *Boundary condition*

Establishing suitable boundary conditions is an essential step in the modeling procedure. In this particular case, where glass covers the slope box model, establishing suitable boundary conditions is also essential. To represent the enclosure of the model, five closed boundary conditions are used, which effectively restrict the flow of materials and forces through these barriers. This configuration closely resembles the situation that occurs in real life when the slope is limited inside a model box. Where the slope material interacts with the model box, an interface condition is also applied. In order to accurately simulate the interaction between the slope material and its container, which affects things like friction and movement at the border, this is crucial. Three boundary conditions are set on top of the slope model to imitate infiltration during rains. These prerequisites are essential for correctly simulating the effects of precipitation-derived water on soil, especially with regard to soil stability and behavior. Figure 5 displays the created model following the boundary condition.

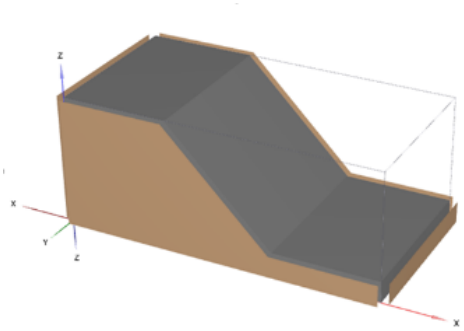

Figure 5: Applied boundary condition

2.2.4. *Vegetation inputs*

During the modeling process, node-to-node anchors were used to replicate the existence of plants on the slope. This method effectively demonstrates how plant or tree roots can strengthen soil and enhance slope stability. 153 nodes were arranged in this configuration, each positioned 10 centimeters apart, with a tensile strength of 29.72 MPa for shrubs [42]. The nodes are elastoplastic model with an EA of 29.72*10^3 KN. During the calculations the maximum stress value on the node is 28.15 MPa, that's below the plastic limit of the node anchors, indicating that the stress is within the material's elastic range and thus within safe operational limits. This configuration of nodes, evenly spaced, guarantees a continuous depiction of vegetation along the incline. The node-to-node anchor system functions similarly to roots, offering extra support and resistance to soil movement. This is crucial for assessing how vegetation affects the slope's stability. The nodes on the slope model are can be seen in the figure 6.

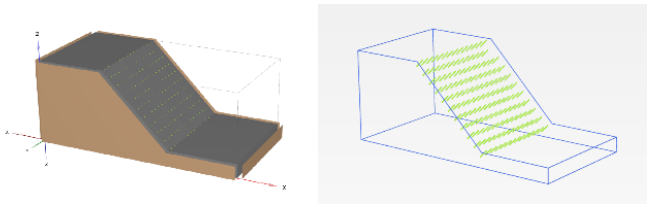

Figure 6: Distributed node anchors on the slope

2.2.5. *Drawdown condition*

The Plaxis model simulates a specific water level fluctuation in the flow condition scenario to analyze the impact of rapid drawdown on the slope. The model is initially set with a water level of 0.8 meters to simulate a high-water scenario. This simulation focuses on the swift decrease of the water level, which is intended to rapidly go from 0.8 meters to 0.4 meters. The quick decline will last for around 6 hours, allowing for a realistic evaluation of the slope's reaction to the sudden water level shift. This brief timeframe is crucial for grasping the immediate impact on the slope's stability, since swift drawdown conditions can greatly change the stress distribution within the slope, possibly resulting in instability or failure. Plaxis model showing the water level is illustrated in the figure 7.

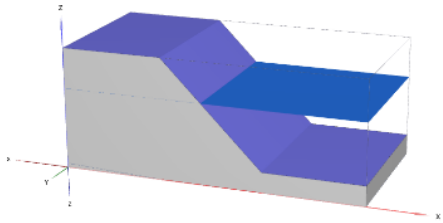

Figure 7: Assigned water level on the slope model

2.2.6. *Phases*

The Plaxis model was constructed in stages to simulate various situations and examine their effects on the slope's stability:

- Initial Phase: The calculation type was set to 'gravity loading' for this phase. This setting is important for establishing the initial stress conditions in the model, simulating the natural gravitational forces acting on the slope.
- Safety Phase: This phase was included to determine the initial factor of safety. Setting up a safety phase helps in assessing the stability of the slope under the initial, undisturbed conditions.
- Rainfall Phase: The time for this phase was set to 0.3 days, simulating an 8-hour rainfall event. The calculation type was 'Fully coupled flow deformation (FCFD)', a crucial setting for realistically simulating the interaction between the soil and the water flow during heavy precipitation. The rainfall intensity was set at 0.72 meters per day (equivalent to 30mm per hour), to mimic a significant rainfall event.
- Safety Phase for Rainfall Analysis: Following the rainfall simulation, another safety phase was set to analyze the factor of safety of the model after the rainfall. This helps in understanding how the slope's stability is affected by the added water from the rainfall. Ignored suction has been used for this phase.
- Drawdown Analysis: The calculation type for this phase was again 'fully coupled flow deformation (FCFD)'. Precipitation was turned off, and the model was adjusted to simulate a water level of 0.8 meters. This setup is used to allow the model to experience drawdown by assigning a flow function that reduces the water head to 0.4 meters, replicating a rapid decrease in water level.
- Safety Phase for Drawdown: Finally, a safety phase was set to analyze the factor of safety for the drawdown analysis. Ignored suction has been used for this phase. This phase is critical for evaluating the stability of the slope post-drawdown, an essential aspect in understanding the impacts of rapid changes in water level on slope stability.

Each of these phases plays a vital role in comprehensively analyzing the different aspects that affect the stability of the slope, from initial conditions to extreme weather events and rapid environmental changes.

3. Results

3.1. *Initial stage*

In the initial phase of the analysis, it is observed how the land is shifting or changing shape. The image clearly shows this happening at the bottom end of the slope. This is common because the toe of a slope often bears a lot of the load and is where movement typically starts if things are going to shift. It's a critical zone where initial movements are most likely to be detected. Numerically, the factor of safety is calculated to be 3.22 with gravity loading. When assessing the vegetated slope, the analysis follows a similar pattern of stability. However, there is a slight increase in the numerical value of the factor of safety, recorded at 3.3. This increment, although marginal, suggests a slightly enhanced stability in the vegetated area compared to the non-vegetated section. The displacement prediction and safety factor comparison for the initial safety phase is show in the figure 8.

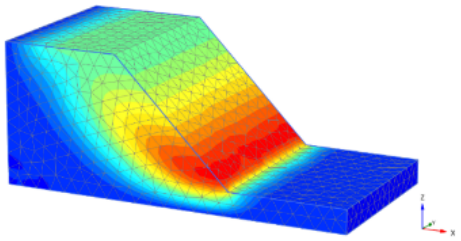

Figure 8: Initial Safety factor phase displacement

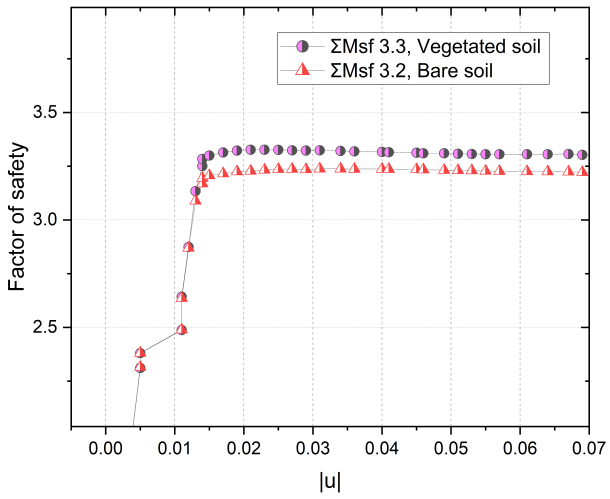

Figure 9: initial phase safety factor comparison

3.2. *Effect of rainfall*

For bare soil, during the 30mm/h rainfall phase of the analysis, observations confirm the initial predictions: the displacement indeed begins at the slope toe. As the rainfall

continues, this deformation isn't just confined to the bottom; it gradually works its way up the slope. Can be seen in the figure 10. The maximum calculated displacement of the slope is 14.7mm. This progression is typical when the lower portions of a slope become saturated and less stable, causing the upper sections to also become more susceptible to movement. Although from the laser scanner, the observed displacement during the experiment were much larger varying from 10mm to 0.21m with a mean displacement of 82mm. This disparity suggests that while the Mohr-Coulomb model(MCM) provides a foundational understanding, it may benefit from refinement. The incorporation of a different behavior law, such as the Hardening Soil Model (HSM), could potentially offer a more precise evaluation of slope displacement. The HSM, which accounts for soil hardening under loading and unloading conditions, might provide a closer alignment between the numerical predictions and the observed data. A brief analysis with HS model has been done to confirm this theory. The maximum displacement in this analysis is 51.2mm, which is higher than the displacement calculated using the MC model. It is also close to the mean displacement observed with the laser scanner shown in figure 12.

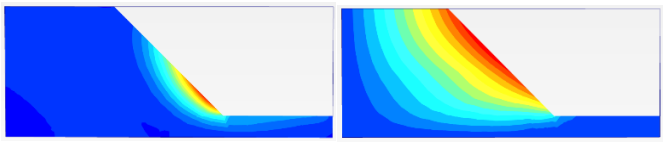

(a) (b)

Figure 10: displacement profile during the rainfall (FCFD) phase where (a) beginning of the phase, (b) end of the phase.

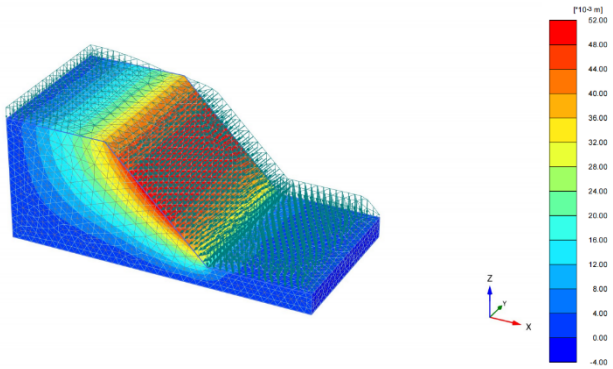

Figure 11: HS model displacement during rainfall (FCFD) phase

The deviatoric strain diagram included in the figure 13 and 14 serves as a detailed visual cue for understanding the shear strain within the landslide body. Essentially, this diagram offers a map of how the soil within the slope is being distorted by the shear forces at play. The size of the shapes in the diagram correlates to the magnitude of shear strain—the larger the shape, the greater the strain. Meanwhile, the area covered by these shapes gives us an idea of where a potential landslide might occur, indicating the probable extent and reach of the sliding surface.

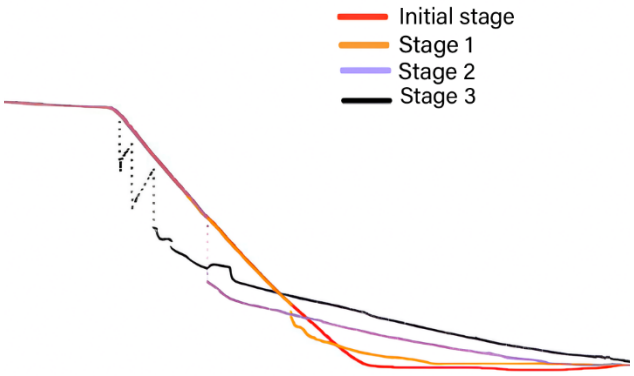

Figure 12: Contour point cloud from laser scanner

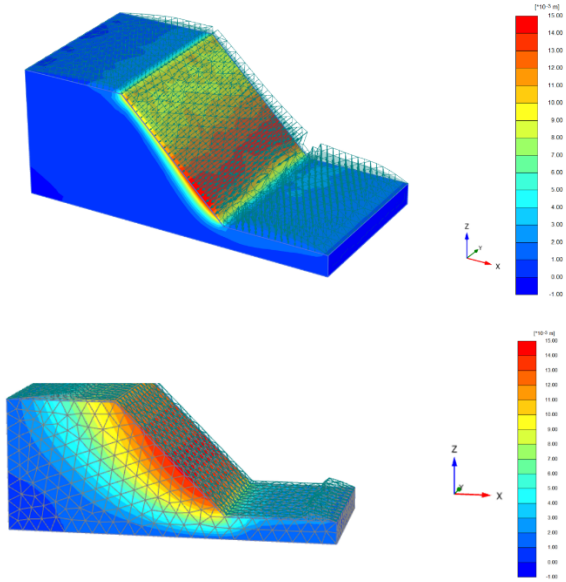

Figure 13: Displacement during rainfall (FCFD) phase.

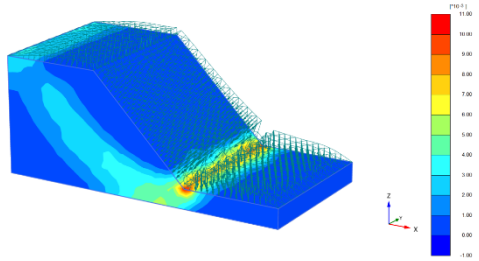

Figure 14: Incremental distribution diagram of slope deviator strain.

The patterns of displacement and deformation observed during the rainfall (FCFD) phase align with the actual erosion seen in the slope model box that can be seen in the laser scanner diagram from figure 12. The progression of movement starting from the slope toe and advancing upward reflects the real-life erosion process can be seen in figure 10. It is comparable with the beginning of the phase to the orange line in figure 12 that is beginning of the deformation observed during the experiment. The deviatoric strain diagram provided a predictive insight into the slope's response to rainfall (shown in figure 15), which turned out to be consistent with the physical erosion seen in the model box.

Figure 15: laboratory slope erosion during rainfall

During the rainfall phase, the factor of safety is calculated to be 1.007 as shown in figure 16. A huge drop from the initial phase. the factor of safety value of 1.007 observed during the rainfall phase indicates that the slope is barely stable, existing in a state of near-equilibrium. This value represents a precarious balance, where the strength of the slope is only slightly greater than the applied stresses. Given this marginal stability, it's understandable why a collapse occurred during the experiment. The rainfall introduces additional variables that negatively impact slope stability, such as reducing soil strength and increasing weight through saturation. These factors, combined with the already minimal safety margin, make the slope highly susceptible to failure.

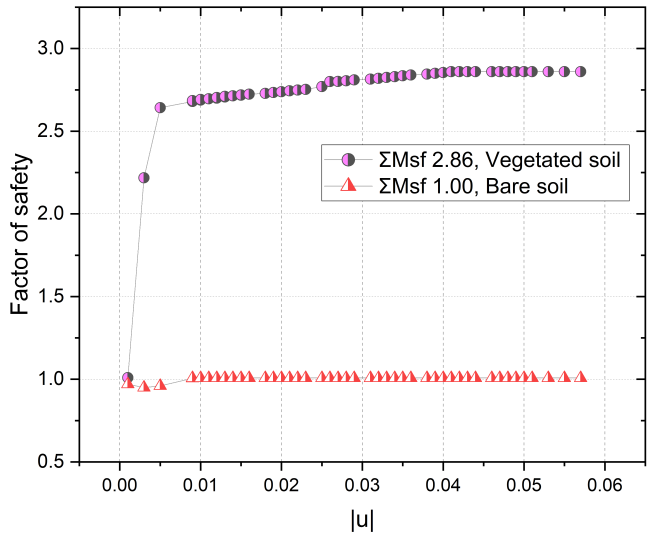

Figure 16: Rainfall phase safety factor comparison.

For vegetated soil, the numerical model indicated minimal displacement during the rainfall phase, which aligns well with the actual experimental observations. Also, the safety factor increased to 2.86. The calculated maximum displacement is 5.2mm, more than 64% decrease from the bare soil analysis. This suggests that the vegetation effectively reinforced the soil, through root systems that helped to bind the soil particles together and distribute the water flow, mitigating the impact of erosion.

The study combined practical experiments and numerical analysis to explore the behavior of pore water pressure (PWP) at various locations. Utilizing sensors, PWP data was gathered, revealing noticeable variations across different points. Specifically, the maximum PWP values recorded by different sensors for bare soil were 4.5, 1.3, 3.8, 0.16, 0.06, 1.28, 0.04, and 0.45, respectively. A notable finding was that the sensor placed mid-slope registered a maximum PWP of 3.8 kPa. This result was particularly interesting because it closely aligned with the peak values predicted by our numerical model, shown in figure 18. For vegetated soil, the sensor data for maximum pwp were 4.89, 5.16, 6.11, 6.20, 1.75, 1.54, 2.14 and 1.36, respectively. The simulated value that closely aligned with the data is 1.68 kPa and 1.74 kPa, shown in figure 19. The observations also indicated that the numerical model tended to simplify the complexity of real-world data. This simplification was evident in the formation of a linear curve in the model, contrasting with the more varied readings from the physical sensors.

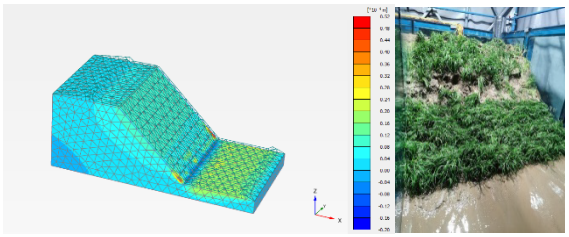

Figure 17: Displacement during rainfall (FCFD) for vegetation induced slope.

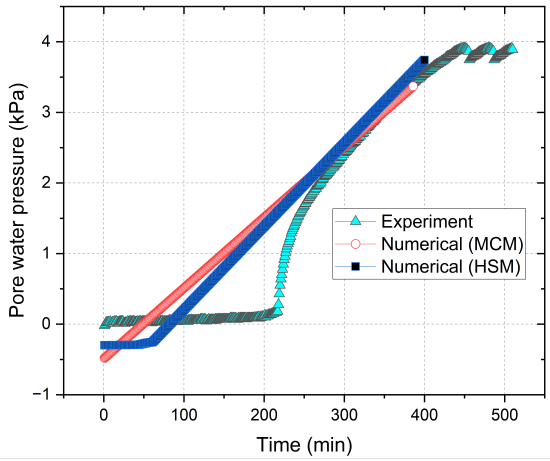

Figure 18: Bare soil pore water pressure comparison.

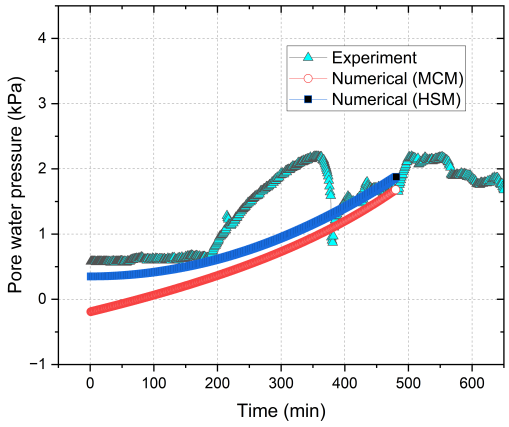

Figure 19: Vegetated soil pore water pressure comparison.

From the sensors volumetric water content data was also gathered. For bare soil, the max value was ranged between 35.1% to 41.5%. From numerical model the max value was 40%, as shown in figure 20 compared to one sensor data. For vegetated soil, max sensor data ranged between 38.8% to 40.9%. numerical model for both MC

model and HS model gave similar assumption. So it is showed as one, as shown in figure 21.

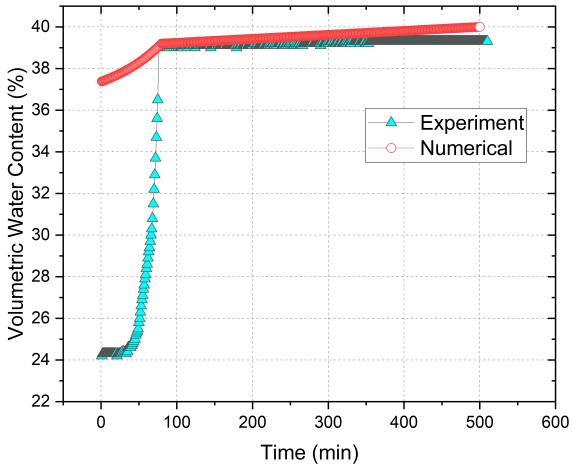

Figure 20: Bare soil volumetric water content comparison.

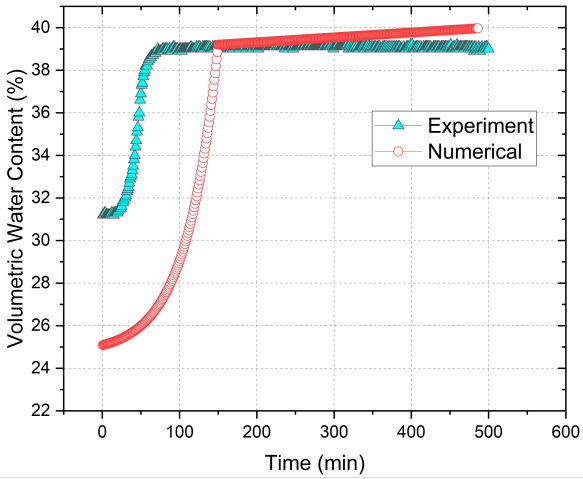

Figure 21: Vegetated soil volumetric water content comparison.

3.3. Effect of rapid drawdown

During the rapid drawdown phase, where the water level dropped 0.4 meters over a period of 8 hours, the slope exhibited a distinct pattern of displacement. The maximum displacement occurring in the middle of the slope is a critical observation. This indicates that the middle section was the most affected by the changes in water level, a phenomenon that can be attributed to the rapid reduction in water pressure and the consequent loss of support for the soil particles.

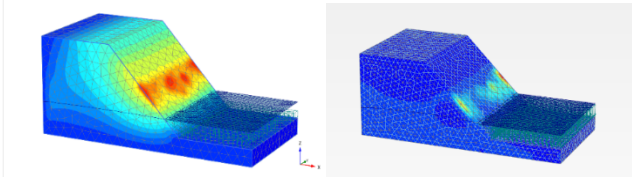

(a) (b)

Figure 22: Displacement during drawdown fully coupled flow deformation phase for (a) bare soil and (b) vegetated soil.

After the rapid drawdown phase, the factor of safety calculated for the slope is 1.3 without vegetation and 2.39 with vegetation.

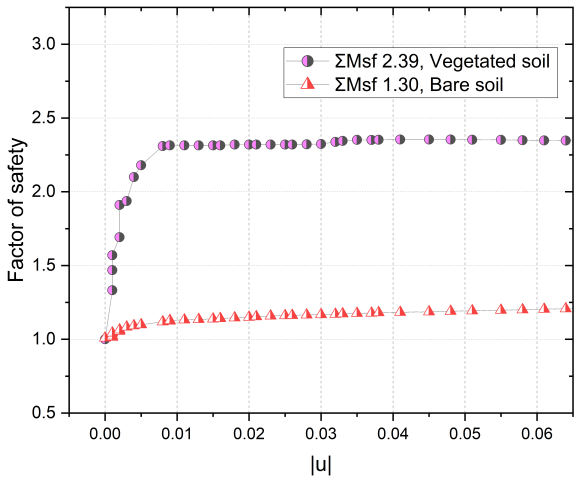

Figure 23: Drawdown phase safety factor comparison.

4. Discussion

The main goal of this study was to investigate riverbank slope stability dynamics, with a specific focus on the impact of water level changes, rainfall, and vegetation. The completion was made by combining empirical data from laboratory experiments with numerical analysis using Plaxis 3D. The methodologies offered a thorough understanding of the complex interactions among different natural factors and how they together affect slope stability.

In the initial phase, the analysis depicted a noticeable shift in the landform, especially at the slope's bottom end, a region typically subjected to significant load and the starting point of movement in case of any instability. The factor of safety was calculated to be 3.22, indicating a stable condition at this stage for gravity loading. For vegetated soil, the factor of safety was slightly higher at 3.3, suggesting that vegetation contributes to the slope's overall stability.

Later, the investigation indicated that during the rainfall phase, displacement started at the slope toe for bare soil. The deformation pattern, beginning at the bottom parts and progressing upwards, corresponds with common reactions to moisture caused by rainfall. The deviatoric strain diagram offered a good depiction of shear strain in the slope, providing predictive information about possible landslide locations. During the observation from the experiment, the diagram closely matches the displacement of the slope. Although from the laser data it can be seen that the actual displacement value was much higher during the experiment than simulation. Later using the Hardening Soil Model, the displacement was higher and close to the laser data than the Mohr-Coulomb Model analysis. The hardening soil model, accounting for non-linear soil behavior and changes in stiffness under different load conditions, offers a more realistic representation of how soil behaves in real-world scenarios. This contrasts with the simpler, linear approach of the Mohr-Coulomb model, which doesn't fully capture

complexities like strain hardening or pressure effects on soil strength. Displacement during the plaxis simulation for vegetated soil decreased by over 64%. The laser cannot scan the soil below the vegetation, that's why it was not used during this experiment. But the plaxis displacement shows the correlation observed during the vegetated slope experiment. For further confirmation, the factor of safety in this phase is 2.86 whereas for bare soil factor of safety is 1, which shows highlights of the critical role of vegetation in reinforcing slope stability under heavy rain conditions. A factor of safety of 1 for bare soil suggests that the slope's strength is just enough to counteract the applied stresses, signifying a threshold condition where any additional stress could lead to failure such as rainfall in this case. In contrast, a factor of safety above 2 for vegetated slopes indicates a much more stable condition.

In comparing the two slope models pore water pressure, it can be seen that the bare soil numerical presents somewhat consistent correlation between experimental data. However, the vegetated soil numerical data revealed a marked variance where notable fluctuations not captured by the smoother numerical model. While it is broadly following the trend, but may not account for certain complex transient conditions that are reflected in the experimental measurements. For volumetric water content, comparing the two graphs depicting volumetric water content over time, both illustrate a characteristic rapid increase followed by a plateau, indicative of approaching saturation. The numerical simulations slightly overestimate the volumetric water content in both. Despite the discrepancies, the consistency of the numerical predictions across both graphs supports their validity in capturing the overall trend of water content changes.

During the rapid drawdown phase, where water levels decreased by 0.4 meters, revealed significant displacement patterns, particularly in the slope's middle section. This phenomenon is attributed to the rapid reduction in water pressure, resulting in less support for the soil particles and subsequent displacement. The factor of safety in this phase for bare soil calculated at 1.3 and 2.39 for vegetated soil. The vegetated soil's strength is more than double the stress acting on it, suggesting a robust level of stability. Vegetation, through its root systems, increases the shear strength of the soil, thereby enhancing its stability. Because the soil is enforced with vegetation, the deformation is minimum.

The study's methodology, while robust, does encounter several limitations that could influence its internal and external validity. Plaxis inevitably involves simplifications and assumptions. These may not fully capture all nuances of real-world scenarios, such as accurate modeling of soil heterogeneity, root-soil interactions, and complex hydrological processes. The laboratory experiments conducted were on a smaller scale. When scaling up these results to real-world scenarios, there might be inaccuracies. The controlled environment of a laboratory cannot perfectly replicate the variable and often unpredictable natural conditions.

The impact of factors like seasonal water level variations and rainfall patterns can differ significantly across various geographic regions. Thus, the study's findings may not encompass the full range of environmental conditions found in diverse settings. The study's approach to understanding the role of vegetation in slope stability may be somewhat generalized. The effects of vegetation can vary greatly depending on species, age, root structure, and health. These limitations highlight the need for cautious interpretation of the study's findings and suggest areas for further research to enhance the understanding and predictive capabilities of slope stability models under various environmental conditions.

5. Conclusion

The study examined the impact of water level fluctuations, rainfall, and vegetation on riverbank slope stability, offering vital insights into the intricate relationship among these natural elements. Empirical evidence and numerical research showed that vegetated slopes are more stable, especially during rains. The study verified the crucial function of vegetation in strengthening soil and reducing erosion, highlighting its significance in slope stability. The study also suggests that using hardened soil in the models yielded more accurate measurements in comparison to real-world data. This indicates the importance of considering soil hardening as a factor in predicting slope stability. This study also emphasizes the influence of water level rapid drawdown and precipitation patterns on slope stability. Quick changes in water levels, especially during drawdown phases, are important elements that affect the mechanical behavior and stability of riverbank slopes.

The study is consistent with other research, highlighting the substantial influence of rainfall on slope instability. Nevertheless, it faces constraints because of the simplifications in the numerical model and the limited scope of laboratory experiments, which may not accurately reflect a wide range of real-world scenarios. The results emphasize the necessity for additional study in geotechnical engineering, particularly in enhancing modeling methods and comprehending the diverse effects of natural elements on slope stability.

Acknowledgement

The research is financially supported by the National Key Research and Development Program of China (No. 2021YFE0194300).

Conflict of Interest

The authors declare no conflict of interest.

References

[1] J.E. Norris, A. Stokes, S.B. Mickovski, E. Cammeraat, R. Van Beek, B.C. Nicoll, A. Achim, Slope stability and erosion control: Ecotechnological solutions, 2008, doi:10.1007/978-1-4020-6676-4.

[2] D. Haque, M.I. Reza, "Parametric Analysis of Slope Stability for River Embankment," *Journal of Advanced Engineering and Computation*, 2020, doi:10.25073/jaec.202043.291.

[3] S. Wen, H. La, C. Wang, "Analysis of influence factors of slope stability," in *Applied Mechanics and Materials*, 2013, doi:10.4028/www.scientific.net/AMM.256-259.34.

[4] R. Hack, D. Alkema, G.A.M. Kruse, N. Leenders, L. Luzi, "Influence of earthquakes on the stability of slopes," *Engineering Geology*, vol. 91, no. 1, 2007, doi:10.1016/j.enggeo.2006.12.016.

[5] H. Rahardjo, T.H. Ong, R.B. Rezaur, E.C. Leong, "Factors Controlling Instability of Homogeneous Soil Slopes under Rainfall," *Journal of Geotechnical and Geoenvironmental Engineering*, vol. 133, no. 12, 2007, doi:10.1061/(asce)1090-0241(2007)133:12(1532).

[6] D. Huang, S.L. Luo, Z. Zhong, D.M. Gu, Y.X. Song, R. Tomás, "Analysis and modeling of the combined effects of hydrological factors on a reservoir bank slope in the Three Gorges Reservoir area, China," *Engineering Geology*, vol. 279, , 2020, doi:10.1016/j.enggeo.2020.105858.

[7] M. Kamran, X. Hu, M.A. Hussain, K. He, A. Nawaz, R. Ali, "Characterizing the Fundamental Controls on Deformation and Stability of an Active Reservoir Landslide, Southwest China," *Polish Journal of Environmental Studies*, vol. 31, no. 4, 2022, doi:10.15244/pjoes/146937.

[8] J. Iqbal, X. Tu, W. Gao, "The impact of reservoir fluctuations on reactivated large landslides: A case study," *Geofluids*, 2019, doi:10.1155/2019/2374236.

[9] Z. Zhou, J. Shen, S. Tang, W. Duan, J. Wang, R. Yang, S. Zheng, F. Guo, "Analysis of weakening law and stability of sliding zone soil in thrust-load-induced accumulation landslides triggered by rainfall infiltration," *Water (Switzerland)*, vol. 13, no. 4, 2021, doi:10.3390/w13040466.

[10] L.L. Zhang, J. Zhang, L.M. Zhang, W.H. Tang, Stability analysis of rainfallinduced slope failure: A review, *Proceedings of the Institution of Civil Engineers: Geotechnical Engineering*, vol. 164, no. 5, 2011, doi:10.1680/geng.2011.164.5.299.

[11] A. Tohari, M. Nishigaki, M. Komatsu, "Laboratory Rainfall-Induced Slope Failure with Moisture Content Measurement," *Journal of Geotechnical and Geoenvironmental Engineering*, vol. 133, no. 5, 2007, doi:10.1061/(asce)1090-0241(2007)133:5(575).

[12] A.B. Fourie, "Predicting rainfall-induced slope instability," *Proceedings of the Institution of Civil Engineers: Geotechnical Engineering*, vol. 119, no. 4, 1996, doi:10.1680/igeng.1996.28757.

[13] W. Wu, "Lulu Zhang, Jinhui Li, Xu Li, Jie Zhang, Hong Zhu: Rainfall-induced soil slope failure: stability analysis and probabilistic assessment," *Acta Geotechnica*, vol. 12, no. 5, 2017, doi:10.1007/s11440-017-0591-8.

[14] S. Rawat, R. Zodinpuii, B. Manna, K.G. Sharma, "Investigation on failure mechanism of nailed soil slopes under surcharge loading: testing and analysis," *Geomechanics and Geoengineering*, vol. 9, no. 1, 2014, doi:10.1080/17486025.2013.804211.

[15] G. Zhang, Y. Hu, L. Wang, "Behaviour and mechanism of failure process of soil slopes," *Environmental Earth Sciences*, vol. 73, no. 4, 2015, doi:10.1007/s12665-014-3522-0.

[16] G. Tang, J. Huang, D. Sheng, S.W. Sloan, "Stability analysis of unsaturated soil slopes under random rainfall patterns," *Engineering Geology*, vol. 245, , pp. 322–332, 2018, doi:10.1016/J.ENGGEO.2018.09.013.

[17] N.S.B. Nasir Ahmad, F.B. Mustafa, S.@. Y. Muhammad Yusoff, G. Didams, A systematic review of soil erosion control practices on the agricultural land in Asia, *International Soil and Water Conservation Research*, vol. 8, no. 2, 2020, doi:10.1016/j.iswcr.2020.04.001.

[18] P. Sun, G. Wang, L.Z. Wu, O. Igwe, E. Zhu, "Physical model experiments for shallow failure in rainfall-triggered loess slope, Northwest China," *Bulletin of Engineering Geology and the Environment*, vol. 78, no. 6, pp. 4363–4382, 2019, doi:10.1007/S10064-018-1420-5/METRICS.

[19] Q. Zhang, Z. Luo, Y. Chen, Z. Wang, "Physical Model Experiments on Failure Mechanism on Slopes of Weathered Basalt Soils during Heavy Rainfall Events," *Materials*, vol. 16, no. 2, 2023, doi:10.3390/ma16020832.

[20] A. Gurnell, "Plants as river system engineers," *Earth Surface Processes and Landforms*, vol. 39, no. 1, 2014, doi:10.1002/esp.3397.

[21] P.M. Rowiński, K. Västilä, J. Aberle, J. Järvelä, M.B. Kalinowska, How vegetation can aid in coping with river management challenges: A brief review, *Ecohydrology and Hydrobiology*, vol. 18, no. 4, 2018, doi:10.1016/j.ecohyd.2018.07.003.

[22] T.H. Wu, "Effect of vegetation on slope stability," *Transportation Research Record*, vol. 965, , pp. 37–46, 1984.

[23] Y. Chok, W. Kaggwa, "Modelling the effects of vegetation on stability of slopes," in *Australia-New Zealand Conference on Geomechanics*, 391–397, 2004.

[24] M. Cecconi, P. Napoli, V. Pane, "Effects of soil vegetation on shallow slope instability," *Environmental Geotechnics*, vol. 2, no. 3, 2015, doi:10.1680/envgeo.13.00110.

[25] W.L. Wieder, S.A. Shoop, State of the knowledge of vegetation impact on soil strength and trafficability, *Journal of Terramechanics*, vol. 78, , 2018, doi:10.1016/j.jterra.2018.03.006.

[26] R. Oorthuis, J. Vaunat, M. Hürlimann, A. Lloret, J. Moya, C. Puig-Polo, A. Fraccica, "Slope orientation and vegetation effects on soil thermo-hydraulic behavior. An experimental study," *Sustainability (Switzerland)*, vol. 13, no. 1, 2021, doi:10.3390/su13010014.

[27] H.Z. Oo, L.Z. Ai, Z. Qiu, "Numerical Analysis of River Bank Slope Stability During Rapid Drawdown of Water Level," *Study of Civil Engineering and Architecture*, vol. 2, no. 4, 2013.

[28] N.A. Taha, M.S.M. Shariff, M.A. Ladin, "Case Study on Analyses of Slope Riverbank Failure," *Modelling and Simulation in Engineering*, vol. 2022, , 2022, doi:10.1155/2022/1965224.

[29] W. Geng-sun, "THE PROGRESSIVE FAILURE OF SLOPE AND THE STABILITY ANALYSES," *Chinese Journal of Rock Mechanics and Engineering*, vol. 19, no. 1, pp. 29–33, 2000.

[30] Y. Li, C. He, "Research Progress on Dynamic Stability of Layered Rock Slope," in *IOP Conference Series: Earth and Environmental Science*, 2021, doi:10.1088/1755-1315/760/1/012058.

[31] M. Sazzad, F.I. Rahman, A.A. Mamun, "Effects of Water-Level Variation on the Stability of Slope By Lem and Fem," *International Conference on Civil Engineering for Sustainable Development*, no. February, 2016.

[32] Y. Lu, Y. Tan, X. Li, "Stability analyses on slopes of clay-rock mixtures using discrete element method," *Engineering Geology*, vol. 244, , 2018, doi:10.1016/j.enggeo.2018.07.021.

[33] N.M. Saim, A. Kasa, "Comparative Analysis of Slope Stability using Finite Element Method (FEM) and Limit Equilibrium Method (LEM)," in *2023 IEEE 14th Control and System Graduate Research Colloquium, ICSGRC 2023 - Conference Proceeding*, 2023, doi:10.1109/ICSGRC57744.2023.10215453.

[34] Y.W. Zeng, W.M. Tian, "Slope stability analysis by combining FEM with limit equilibrium method," *Yanshilixue Yu Gongcheng Xuebao/Chinese Journal of Rock Mechanics and Engineering*, vol. 24, no. SUPPL. 2, 2005.

[35] A. Kaur, R.K. Sharma, "SLOPE STABILITY ANALYSIS TECHNIQUES: A REVIEW," *International Journal of Engineering Applied Sciences and Technology*, vol. 1, , 2016.

[36] A. Burman, S.P. Acharya, R.R. Sahay, D. Maity, "A comparative study of slope stability analysis using traditional limit equilibrium method and finite element method," *Asian Journal of Civil Engineering*, vol. 16, no. 4, 2015.

[37] G.M.M. Alam, K. Alam, S. Mushtaq, M.N. Khatun, W. Leal Filho, Strategies and barriers to adaptation of hazard-prone rural households in Bangladesh, 2018, doi:10.1007/978-3-319-64599-5_2.

[38] J.P. Aryal, T.B. Sapkota, D.B. Rahut, T.J. Krupnik, S. Shahrin, M.L. Jat, C.M. Stirling, "Major Climate risks and Adaptation Strategies of Smallholder Farmers in Coastal Bangladesh," *Environmental Management*, vol. 66, no. 1, 2020, doi:10.1007/s00267-020-01291-8.

[39] Plaxis, General Information Manual, 2024.

[40] Plaxis, Reference Manual 3D, 2024.

[41] J.T. Bowers, M.C. Webb, J.L. Beaver, "Soil Parameters for Design with the 3D PLAXIS Hardening Soil Model," *Transportation Research Record*, 2019, doi:10.1177/0361198119851723.

[42] F. Ali, "Use of vegetation for slope protection: Root mechanical properties of some tropical plants," *International Journal of Physical Sciences*, vol. 5, no. 5, 2010.

JENRS

Received: 25 January, 2024, Revised: 02 April, 2024, Accepted: 05 April, 2024, Online: 30 April, 2024

DOI: https://doi.org/10.55708/js0304004

Computational and Bioinformatics Approaches for Identifying Comorbidities of COVID-19 Using Transcriptomic Data

Shudeb Babu Sen Omit*[1], Md Mohiuddin[2], Salma Akhter [3], Md. Hasan Imam[1], A. K. M. Mostofa Kamal Habib[4], Syed Mohammad Meraz Hossain[5], Nitun Kumar Podder[6]

[1]Institute of Information Technology, Noakhali Science and Technology University, Noakhali, 3814, Bangladesh

[2]Department of Mechanical Engineering, Chittagong University of Engineering and Technology, Chattogram, 4349, Bangladesh

[3]Department of Environmental Science and Disaster Management, Noakhali Science and Technology University, Noakhali 3814, Bangladesh

[4]National Skills Development Authority, Dhaka, Bangladesh

[5]Department of Information and Communication Technology, Dhaka, Bangladesh

[6]Department of Computer Science and Engineering, Pabna University of Science and Technology, Pabna, 6600, Bangladesh

*Corresponding author: Shudeb Babu Sen Omit, Email: omit.shen@gmail.com

ABSTRACT: Comorbidity is the co-existence of one or more diseases that occur concurrently or after the primary disease. Patients may have developed comorbidities for COVID-19 that cause harm to the patient's organs. Besides, patients with existing comorbidities are at high risk, since mortality rates are strongly influenced by comorbidities or former health conditions. Therefore, we developed a computational and bioinformatics model to identify the comorbidities of COVID-19 utilizing transcriptome datasets of patient's whole blood cells. In our model, we employed gene expression analysis to identify dysregulated genes and curated diseases from Gold Benchmark databases using the dysregulated genes. Subsequently, Tippett's Method is used for COVID-19's P-value calculation, and according to the P-value, Euclidean distances are calculated between COVID-19 and the collected diseases. Then the collected diseases are ordered and clustered based on the Euclidean distance. Finally, comorbidities are selected from the top clusters based on a comprehensive literature search. Applying the model, we found that acute myelocytic leukemia, cancer of urinary tract, body weight changes, abdominal aortic aneurysm, kidney neoplasm, diabetes mellitus, and some other rare diseases have correlation with COVID-19 and many of them reveal as comorbidity. Since comorbidities are in conjunction with the primary disease, thus similar drugs and treatments can be used to recover both COVID-19 and its comorbidities by further research. We also proposed that this model can be further useful for detecting comorbidities of other diseases as well.

KEYWORDS: COVID-19, Comorbidity Identification, Transcriptomic Data, Tippett's Method, Euclidean Distance

1. Introduction

COVID-19 is an infectious disease first reported in December 2019 in Wuhan, Hubei Province, China, caused by severe acute respiratory syndrome coronavirus 2 (SARS-CoV-2). Through direct contact or droplets from the infected person's respiratory system, COVID-19 is spread between individuals [1], [2]. Consequently, COVID-19 has spread to almost all countries around the world, and on 11 March 2020, the World Health Organization (WHO) declared it a global pandemic. The WHO estimates that COVID-19 causes more than 180 million confirmed cases and 4 million deaths worldwide. This death is often caused by the underlying comorbidities of COVID-19, and the severity of the disease is increased by these existing conditions, as the comorbidities are correlated with morbidity and mortality [3] — [5]. In addition, COVID-19 indirectly impacts damage to organ systems and organs of the human body, which is also resulting in death [6] — [9]. It is therefore vital to develop a computation-based approach that can detect the comorbidities of COVID-19 so that early protection, prevention, and treatment can be implemented.

There have been several studies performed to identify COVID-19 comorbidities. In [10], the authors found that hypertension, diabetes, cardiovascular diseases, and

chronic kidney disease are the most common comorbidities of COVID-19. In [11], cardiovascular disease and chronic respiratory disease are the riskiest comorbidities observed by the authors. Another study performed in [12] and the authors showed that hypertension, diabetes, obstructive pulmonary disease, cardiovascular disease, and cerebrovascular disease are the risk factors associated with COVID-19. Moreover, according to [13], hypertension, chronic cardiovascular disease, diabetes, and chronic cerebrovascular disease have a high percentage in COVID-19 patients. Besides, in [14], the authors reported hypertension, diabetes mellitus, cerebrovascular, cardiovascular disease, kidney disease, etc. as comorbidities of COVID-19. A similar analysis by the authors of [15] also reported that hypertension, diabetes, obesity, asthma, etc. are the comorbidities in hospitalized COVID-19 patients.

We found that a considerable number of works identifying the comorbidities of COVID-19 are based on literature-driven meta-analyses and some of them are discussed in the literature review section. Therefore, we have performed a computational and bioinformatics-based approach to detect COVID-19's comorbidities

Our analysis was based on transcriptomic data derived from blood samples of COVID-19 patients and healthy individuals. Then we analyzed the dataset with the GEO2R (https://www.ncbi.nlm.nih.gov/geo/geo2r/) tool and identified up and down-regulated genes. As a result of these dysregulated genes, we compiled a list of associated diseases from Gold Benchmark databases. Then the P-value of COVID-19 is calculated, as described in the following sections. After that, Euclidean distance is used to measure how close the collected diseases are to COVID-19. The Euclidean distances are calculated between COVID-19's P-value and the Gold Benchmark diseases' P-value. Consequently, the short Euclidean distances mean more proximity of diseases with COVID-19. Next, we organized the collected diseases in small to large orders according to the Euclidean distance. Then the diseases of similar Euclidean distance are clustered from top to bottom of the organized list. In our final step, we selected the comorbidity from the top clusters.

The main contributions of our paper are as follows:

- As a result of conducting our analysis on genetic data, we avoided the influences of literature-driven type biases.
- As we have used a transcriptomic dataset of the whole genome from the blood sample, some novel findings can potentially be revealed as the comorbidity of COVID-19.
- Our pipeline is capable of generating automated results provided input dataset.
- Finally, if the transcriptomic dataset exists, it is possible to apply the technique swiftly to different diseases.

The rest of the paper is structured as follows: Section II describes related previous works and their shortcomings; Section III depicts the proposed pipeline outlining our methodology and analysis. Section IV discusses the outcomes and validation. Section V concludes our paper and introduces future extensions of the work.

2. Literature Review

According to the World Health Organization, there have been 170,426,245 confirmed cases, including 3,548,628 deaths due to the COVID-19 pandemic globally as of 1 June 2021. The number of infected people and deaths is increasing rapidly and this mortality, infection, and severity are getting more dangerous because of existing comorbidities and underlying health conditions [16] — [18]. Hence it is important to identify the comorbidities or risk factors to reduce severe COVID-19 progression. Some COVID-19 comorbidities associated research works are presented as follows:

A meta-analysis of the published global literature was conducted by the authors of [19] by combining clinical data with comorbidity details, they were able to identify significant COVID-19 comorbidities. They found chronic kidney disease, type-2 diabetes, malignancy, hypertension, cardiovascular disease, etc. as the most significant comorbidities associated with COVID-19; working with published articles and aggregated clinical cohort data there is a possibility of biases.

By reviewing the literature the authors of [20] selected angiotensin-converting enzyme 2 (ACE2), transmembrane protease serine 2 (TMPRSS2), and basigin (BSG) as viral attack receptors and obtained PPI data from bioinformatics and system biology databases. They identified 59 proteins that interact with SARS-CoV-2 proteins and using the identified proteins they collected diseases named as comorbidities from DisGeNet [21], OMIM [22], ClinVar [23], and PheGenI [24] databases. They also selected 79 diseases from a list of diseases that are associated with 30 proteins selected from 59 proteins and the selections are not clear.

In [25], the authors explored the gene expression patterns from 30 array-based acute, chronic, and infectious gene expression datasets by meta-analysis. They observed the genes of the diseases are correlated and using literature mining they identified 78 genes which include receptors, and proteases of SARS-CoV-2 pathogenesis. Their findings also indicated that COVID-19 is susceptible to leukemia, nonalcoholic fatty liver disease, psoriasis, diabetes, and pulmonary arterial hypertension as comorbidities, through co-expression analysis of genes, pathways enrichment analysis, and significant enrichment of pathways.

Using data from preexisting diagnoses and hospitalized COVID-19 patients, the authors of [26] identified COVID-19 risk factors using the UK Biobank.

Using logistic regression model, they estimated risks for each comorbidity from the existing comorbidities and found that males, people of black ethnicity, and no educational qualification people have a higher risk of COVID-19.

A study by the authors of [27] attempted to relate COVID-19 to breast cancer, colon cancer, kidney cancer, liver cancer, bladder cancer, prostate cancer, thyroid cancer, and lung cancer. Their findings identified dysregulated genes, pathways, gene ontologies, and associations and interactions between cancers and COVID-19. They marked the cancers as comorbidities based on their association and interaction with COVID-19. Anteriorly they selected the diseases, then COVID-19 is associated with the selected diseases.

In [28], the authors selected five illnesses: kidney, liver, diabetes, lung, and cardiovascular illness from the literature as comorbidities and examined their potential association with COVID-19. First, they identified the common genes of the comorbidities, then they conducted phenotype enrichment analysis and pathway enrichment analysis using the shared genes; they also identified common pathways between COVID-19 and the comorbidities and investigated the association of the pathways with COVID-19 itself.

By the authors of [29], laboratory-confirmed COVID-19 studies were meta-analyzed. In COVID-19 patients, the spread of comorbidities was evaluated, and the risk factor was identified. They found that older and male patients are more susceptible to COVID-19; also, they marked hypertension, diabetes, cardiovascular and followed by respiratory system diseases as prevalent risk factors from the literature.

Based on pooled proportion, the authors of [30] performed a systematic review and meta-analysis of comorbidities prevalence, severity, and mortality concerning age, gender, and geographic areas. They observed a high prevalence of comorbidities in the USA, the highest severity in Asia with the highest mortality in Europe and Latin American region; chronic kidney disease is highly responsible for disease severity and cerebrovascular accident, chronic kidney disease, and cardiovascular disease for mortality of COVID-19 patients. By reviewing the articles, they also got higher severity in female patients and mortality in older and male patients.

We analyzed the COVID-19 dataset in a systematic way to figure out the comorbidity.

P-value combination is very common in bioinformatics [31] and there are diverse methods for combining P-values from multiple statistical tests such as Brown's Method [31], Fisher's Method [32], Truncated Product Method [33], Stouffer's Method [34], Tippett's Method [35], Bonferroni Method [36], Weighted Z-test [37], Z-transform Test [38], Liptak Test [39], Sidak Test [40], Simes' Test [40], Gamma Distribution [41] etc. For different situations and datasets, different methods are powerful and suitable [41]; in our case, Tippett's Method is decent, and using Tippett's Method we got COVID-19's P-value. In later sections, a discussion about COVID-19's P-value is there and after getting the P-value we did our further analysis.

3. Methods and Analysis

3.1. Covid-19 Dataset and Geo2r Analysis

For our investigation, we collected the dataset from National Center for Biotechnology Information (NCBI) (https://www.ncbi.nlm.nih.gov/) with accession number GSE166552 which is a microarray dataset prepared from blood samples of COVID-19 patients and healthy people. Initially, we analyzed the gene expression dataset with a web-based GEO2R tool, setting force normalization [42], precision weight (vooma) [43], and Benjamini & Hochberg (False discovery rate) [44] and comparing the transcriptomic profile of infected and control samples incorporating GEOquery [45], limma [46], and umap [47] R packages. The dataset comprises columns such as gene ID, adjusted P-value, P-value, Log2 fold change (logFC), gene sequence, and gene symbol. It was observed that certain cells within the gene symbol column were identified as missing values. Consequently, data related to these missing gene symbols were filtered out during the preprocessing phase. After preprocessing the dataset, we worked on the following analysis.

3.2. Dysregulated Genes and Disease Collection

To identify the comorbidities, statistically significant dysregulated (up-regulated and down-regulated) genes (DGs) are selected as follows:

$$DGs = \begin{cases} Up-regulated, P-value \le 0.05 \,\&\, log\,FC \ge 1.0 \\ Down-regulaed, P-value \le 0.05 \,\&\, log\,FC \le 1.0 \end{cases} \quad (1)$$

Afterwards, more than 20,000 diseases associated with the selected DGs were obtained from several Gold Benchmark databases, including DisGeNET [21], ClinVar 2019 [23], PheWeb 2019 [48], dbGap [49], OMIM Disease [50], OMIM Expanded [50], Rare Diseases AutoRIF ARCHS4 Predictions [51], Rare Diseases GeneRIF ARCHS4 Predictions [51], Rare Diseases GeneRIF Gene Lists [51], Rare Diseases AutoRIF Gene Lists [51] and GWAS Catalog 2019 [52].

3.3. Covid-19's P-value Calculation

The dataset used in this study was derived from COVID-19 patients and comprises a large number of genes with individual P-values. Our objective is to obtain a single P-value from the dataset representing the P-value of COVID-19. Thus, we combined all the genes' P-values to get a single P-value that is considered COVID-19's P-value using Tippett's Method as follows:

$$p_c = 1 - (1 - min(p_1, p_2, p_3 \ldots p_i))^k \quad (2)$$

Where *min* is the minimum function of $P_1, P_2, P_3 ... P_n$ as well as $P_1, P_2, P_3 ... P_n$ denote separate P-values and k is the total number of P-values of the genes of the dataset.

3.4. Euclidean Distance and Disease Order

In our investigation, we calculated the Euclidean distance between the P-value of COVID-19 and all the other individual diseases that were collected using the dysregulated genes. The distance is the absolute value difference of the P-values as follows:

$$E_d = |X_c - Y_i| \quad (3)$$

where X_c denotes the COVID-19's P-value and $Y_i = Y_1, Y_2, Y_3 ... Y_i$ denotes the certain P-value of the collected disease. After getting the Euclidean distance of all other collected diseases from COVID-19, we sorted the collected diseases in ascending order depending on the Euclidean distance.

3.5. Clustering and Comorbidities Selection

In the collected diseases we found that some diseases have the same P-value and as a result, the same Euclidean distance is found for those diseases. We clustered the disease based on the same Euclidean distance of the sorted diseases list from top to bottom maintaining the ascending order. Finally, we select the comorbidities of COVID-19 from the top six clusters.

3.6. Our Proposed Model as An Algorithm

Algorithm: The algorithmic pseudocode to generate the workflows for identification of the comorbidities of COVID-19 as follows:

Input: Microarray dataset with six samples where three samples from COVID-19 patients and another three samples from healthy people.

Output: Related comorbidities of COVID-19.

- Assign patient's samples to the Case and healthy people's samples to the Control group in the GEO2R tool.
- Analyze the dataset using GEO2R by setting force normalization, precision weights, and the Benjamini & Hochberg algorithm.
- Preprocess the dataset after analyzing it by GEO2R.
- Identify up-regulated genes applying $P\text{-}value \le 0.05 \& logFC \ge 1.0$.
- Identify down-regulated genes applying $P\text{-}value \le 0.05 \& log\ FC \le 1.0$.
- Enter the identified dysregulated (up-regulated and down-regulated) genes into the Gold Benchmark databases and gather a list of diseases.
- Calculate COVID-19's P-value using Tippett's method.
- Calculate Euclidean distance from COVID-19 to all other diseases on the list.
- Sort all diseases of the list based on the Euclidean distance in ascending order.
- Cluster all the diseases on the list based on the same Euclidean distance.
- Select correlated comorbidities from the top clusters.

end

The workflow steps of our proposed model are shown in Figure 1.

4. Results and Discussion

After analyzing, preprocessing, and filtering we got 35,011 differentially expressed genes with P-value, adjusted P-value, and fold change value. Then we evicted 1,421 up-regulated genes using a statistical threshold of $P-value \le 0.05$ and absolute Log_2 fold change $(LogFC) \ge 1.0$. Also, we got 2,138 down-regulated genes using $P-value \le 0.05$ and Log_2 fold change $(LogFC) \le 1.0$; a total of 3,559 dysregulated genes were identified. To attain the result, we uploaded a total of 3,559 dysregulated genes in the stated method and analysis section's eleven Gold Benchmark databases of Enrichr [53] which is a web-based gene set enrichment analyzing tool, and got a total of 22,820 common and rare type diseases with P-value, adjusted P-value, gene symbol and many other attributes. Simultaneously we got the P-value of COVID-19 as 0.301041817 by combining the P-values of all 35,011 genes from our filtered dataset using Tippett's method. Next Euclidean distances among the P-value of COVID-19 and 22,820 diseases are enumerated individually and then the total of 22,820 diseases are rearranged in ascending order using the computed Euclidean distances.

Table 1 shows the primary disease and its P-value, top collected diseases, P-values of the top collected diseases, and Euclidean distance from the primary disease to the top collected diseases from left to right. After sorting the collected disease, we got prominent ear, acute myelocytic leukemia, adducted thumb, cancer of urinary tract, increased appetite, malignant neoplasm of vulva, myelodysplastic syndrome with isolated del(5q), nonnuclear polymorphic congenital cataract, chromosome 12 12p trisomy, chromosome 15q trisomy, chromosome 9 monosomy 9p, body weight changes, abdominal aortic aneurysm, kidney neoplasm, diabetes mellitus, and other diseases from top of the total diseases. Many diseases have the same Euclidean distance from COVID-19 and diseases with similar Euclidean distances are retained in the same cluster.

Table 2 represents cluster number, Euclidean distance between COVID-19 and the clusters or clusters' disease, and the disease names in the clusters from left to right. Euclidean distance between cluster 1 and COVID-19 is 0.000149032; in the same way, Euclidean distances are

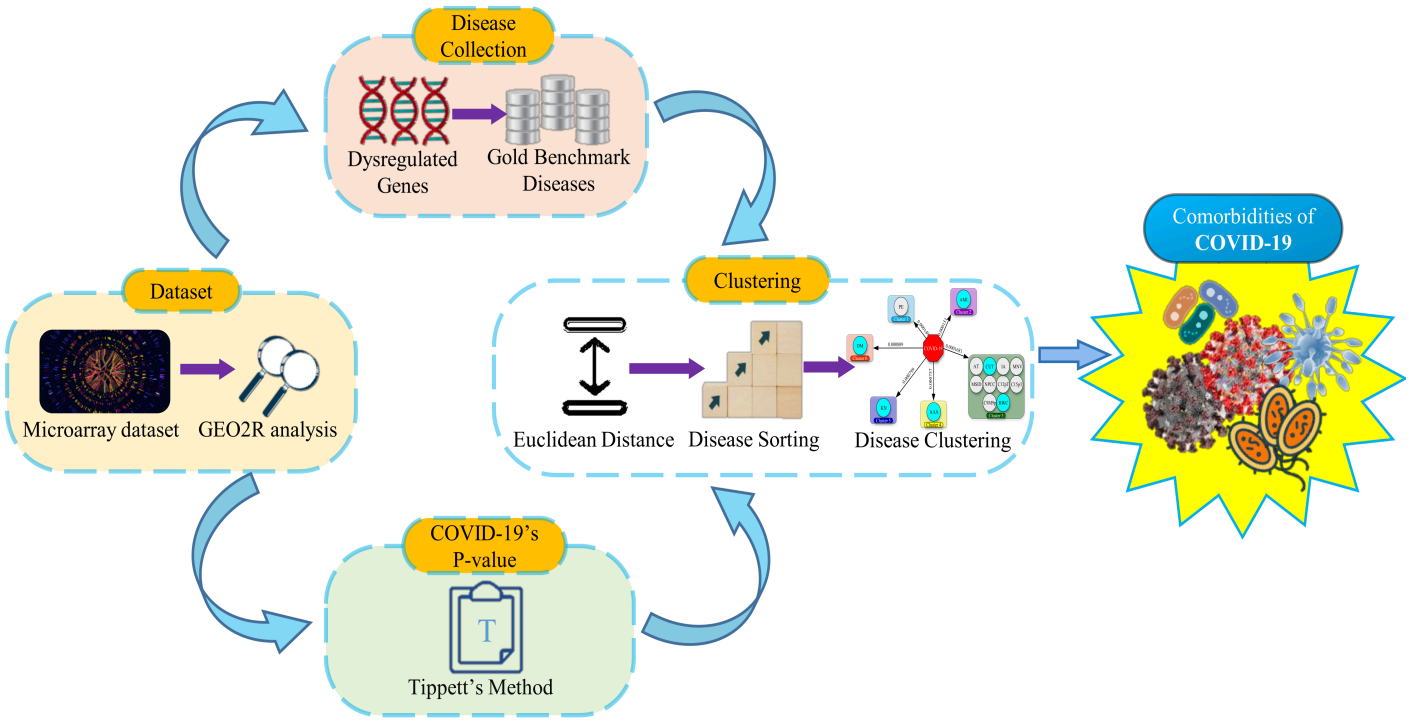

Figure 1: Overview of our computational and bioinformatics experimental approach.

0.0001505, 0.000168149, 0.000756942, 0.000798617 and 0.000808946 among COVID-19 and second cluster, third cluster, fourth cluster, fifth cluster, and sixth cluster.

We clustered the entire 22,820 diseases based on the same Euclidean distance and took the top six clusters. From Figure 2, we see that in cluster no. 1 there is only one disease prominent ear; in cluster 2, only acute myelocytic leukemia is present; cluster 3 contains ten diseases and they are adducted thumb, cancer of urinary tract, increased appetite, malignant neoplasm of vulva, myelodysplastic syndrome with isolated del(5q), nonnuclear polymorphic congenital cataract, chromosome 12 12p trisomy, chromosome 15q trisomy, chromosome 9 monosomy 9p and body weight changes. Again, cluster 4, cluster 5, and cluster 6 hold abdominal aortic aneurysm, kidney neoplasm, and diabetes mellitus.

Finally, we selected comorbidity from our top six clusters. Figure 3 shows that acute myelocytic leukemia is selected as comorbidity from cluster 2, from cluster 3 cancer of urinary tract and body weight changes are selected as comorbidity; abdominal aortic aneurysm, kidney neoplasm, and diabetes mellitus are selected from cluster 4, cluster 5, and cluster 6; only cluster 1 is not considered to select comorbidity as we have not found a relationship between COVID-19 and prominent ear in global research.

We developed a computational and bioinformatics framework to identify the comorbidities of COVID-19 and our model is suitable to obtain the comorbidities of other diseases quickly. As far as we know there is no other such approach to ascertain comorbidities of diseases numerically; there are clinical tests, meta-analysis, and cross-checking tests to determine comorbidities but they

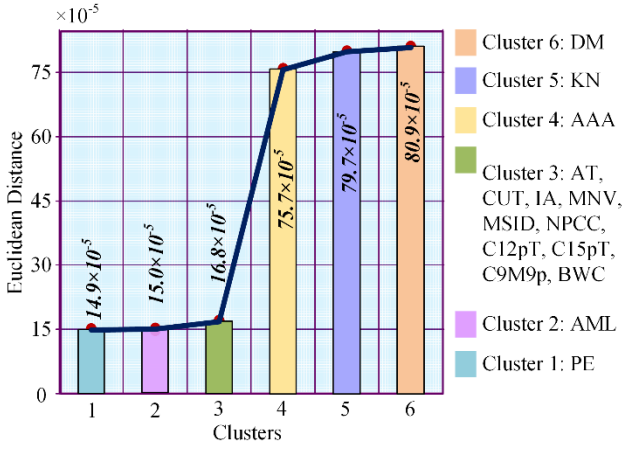

Figure 2: Top six clusters and diseases in each cluster. The legends are cyan color bar for cluster 1 and pink color bar for cluster 2. Similarly, green color, yellow color, violet color, and orange color bars are for cluster 3, cluster 4, cluster 5, and cluster 6. Where PE= Prominent Ear, AML= Acute Myelocytic Leukemia, AT= Adducted Thumb, CUT= Cancer of Urinary Tract, IA= Increased Appetite, MNV= Malignant Neoplasm of Vulva, MSID= Myelodysplastic Syndrome with Isolated del(5q), NPCC= Nonnuclear Polymorphic Congenital Cataract, C12pT= Chromosome 12 12p Trisomy, C15pT= Chromosome 15q Trisomy, C9M9p= Chromosome 9 Monosomy 9p, BWC= Body Weight Changes, AAA= Abdominal Aortic Aneurysm, KN= Kidney Neoplasm and DM= Diabetes Mellitus.

are time-consuming and take much exertion. Acute myelocytic leukemia [54] — [57], cancer of urinary tract [58], [59], body weight changes [60] [61], abdominal aortic aneurysm [62] [63], kidney neoplasm [64] — [66], and diabetes mellitus [67] — [70] are the outcomes of our research where cancer of urinary tract and kidney neoplasm are related to bladder cancer [71], [72]. Moreover, bladder cancer is a post COVID-19 condition [59]. So, there is a chance of ensuing cancer of urinary tract and kidney neoplasm in COVID-19 recovered patients.

Table 1: Summary of results along with the P-value of COVID-19, top collected disease, their P-values and Euclidean distance between COVID-19 and the top collected disease

Primary Disease	P-value of COVID-19	Top Collected Disease	Collected Disease's P-value	Euclidean Distance
COVID-19	0.301041817	Prominent Ear	0.300892784	0.000149032
		Acute Myelocytic Leukemia	0.301192317	0.0001505
		Adducted Thumb	0.301209965	0.000168149
		Cancer of Urinary Tract	0.301209965	0.000168149
		Increased Appetite	0.301209965	0.000168149
		Malignant Neoplasm of Vulva	0.301209965	0.000168149
		Myelodysplastic Syndrome with Isolated del(5q)	0.301209965	0.000168149
		Nonnuclear Polymorphic Congenital Cataract	0.301209965	0.000168149
		Chromosome 12 12p Trisomy	0.301209965	0.000168149
		Chromosome 15q Trisomy	0.301209965	0.000168149
		Chromosome 9 Monosomy 9p	0.301209965	0.000168149
		Body Weight Changes	0.301209965	0.000168149
		Abdominal Aortic Aneurysm	0.300284875	0.000756942
		Kidney Neoplasm	0.3002432	0.000798617
		Diabetes Mellitus	0.301850763	0.000808946

Body weight changes (weight gain or weight loss) is also a post COVID-19 condition [60], [73] and excess weight gain or overweight causes obesity [74].

What we found in our outcomes is also the same in the published literature; thus, we validated our work.

Clinical decision-making and outcomes are significantly affected by comorbidities, which influence treatment strategies and patient management. Research indicates that comorbid conditions complicate the treatment landscape by influencing drug interactions, therapeutic efficacy, and patient compliance [75]. Additionally, comorbidity can complicate the prognosis of primary illnesses, increasing healthcare expenditures [76]. Early detection of comorbidities enables healthcare providers to implement preventive measures and targeted interventions to arrest disease progression and improve patient health [77]. It is also essential to assess and optimize patients with comorbidities before surgery to reduce complications during surgery [78]. Therefore, it is imperative to identify accurate comorbidities early in clinical practice to optimize treatment strategies, improve patient management, and improve health outcomes. Comorbidities that are the result of our work are shown in Figure 4.

Table 2: Disease in each cluster and Euclidean distance from COVID-19 to clusters or clusters' disease

No.	Euclidean distance	Diseases in the cluster
Cluster 1	0.000149032	Prominent Ear
Cluster 2	0.0001505	Acute Myelocytic Leukemia
Cluster 3	0.000168149	Adducted Thumb
		Cancer of Urinary Tract
		Increased Appetite
		Malignant Neoplasm of Vulva
		Myelodysplastic Syndrome with Isolated del(5q)
		Nonnuclear Polymorphic Congenital Cataract
		Chromosome 12 12p Trisomy
		Chromosome 15q Trisomy
		Chromosome 9 Monosomy 9p
		Body Weight Changes
Cluster 4	0.000756942	Abdominal Aortic Aneurysm
Cluster 5	0.000798617	Kidney Neoplasm
Cluster 6	0.000808946	Diabetes Mellitus

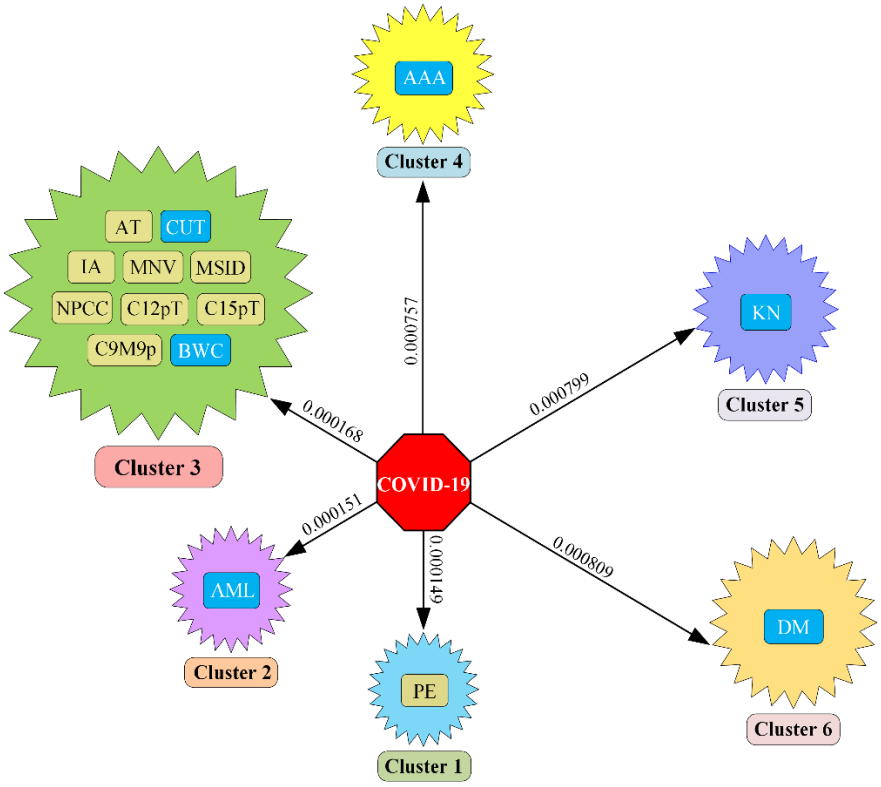

Figure 3: Comorbidities selection from top clusters. The red octagonal node represents COVID-19, 24-point stars represent the clusters, other rounded rectangular-shaped nodes represent the diseases inside the clusters, and cyan color nodes represent the selected comorbidities. Where, PE= Prominent Ear, AML= Acute Myelocytic Leukemia, AT= Adducted Thumb, CUT= Cancer of Urinary Tract, IA= Increased Appetite, MNV= Malignant Neoplasm of Vulva, MSID= Myelodysplastic Syndrome with Isolated del(5q), NPCC= Nonnuclear Polymorphic Congenital Cataract, C12pT= Chromosome 12 12p Trisomy, C15pT= Chromosome 15q Trisomy, C9M9p= Chromosome 9 Monosomy 9p, BWC= Body Weight Changes, AAA= Abdominal Aortic Aneurysm, KN= Kidney Neoplasm and DM= Diabetes Mellitus.

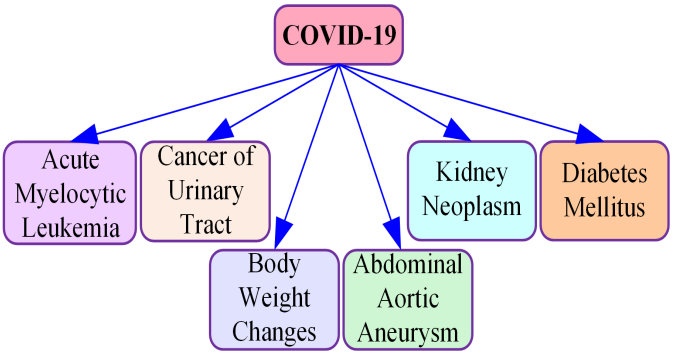

Figure 4: Comorbidities of COVID-19

5. Conclusion

COVID-19's comorbidities increase the disease severity and mortality as well as influence organ damage of the patients; often the patients die due to their main comorbidities. Because of that, it is exigent for medical practitioners to find out the comorbidities of diseases, and in our study, we developed a pipeline that can detect comorbidities of COVID-19 from genetic datasets in a computational and bioinformatics way. We identified *DGs* and diseases related to the *DGs* using the bioinformatics approach as well as detected risk factor diseases linked with COVID-19 as comorbidities from the gathered diseases in a systematic computational way.

In this research, one of the main challenges for us is to find the accurate P-value of COVID-19. We observed that the more accurate COVID-19's P-value gives the more accurate comorbidities as a result. In the future, we will apply other alternative methods to derive the exact P-value of COVID-19. We suggest that our developed approach will assist in the diagnosis of comorbidities of other diseases early if the genetic dataset is available and thus this model will help healthcare systems to reduce the comorbidity diagnosis cost of a disease.

Conflict of Interest

The authors declare no conflict of interest.

Acknowledgment

The assistance for this project is provided by the ICT Division of the Government of the People's Republic of Bangladesh, under Grant number 22FS15614.

References

[1] T. Acter, N. Uddin, J. Das, A. Akhter, "Since January 2020 Elsevier has created a Covid-19 resource centre with free information in English and Mandarin on the novel coronavirus Covid- 19 . The Covid-19 resource centre is hosted on Elsevier Connect , the company ' s public news and information," *Science of the Total Environment Journal*, vol. N/V, no. January, pp. 2–15, 2020.

[2] Coronavirus disease (COVID-19) (no date) Who.int. Available at:

https://www.who.int/health-topics/coronavirus (Accessed: June 20, 2021).

[3] W.J. Guan, W.H. Liang, J.X. He, N.S. Zhong, "Cardiovascular comorbidity and its impact on patients with COVID-19," *European Respiratory Journal*, vol. 55, no. 6, pp. 1069–1076, 2020, doi:10.1183/13993003.01227-2020.

[4] M.J. Hasan, A.M. Anam, S.M.R. Huq, R. Rabbani, "Impact of Comorbidities on Clinical Outcome of Patients with COVID-19: Evidence from a Single-center in Bangladesh," *Health Scope*, vol. 10, no. 1, pp. 1–9, 2021, doi:10.5812/jhealthscope.109268.

[5] H. Ejaz, A. Alsrhani, A. Zafar, H. Javed, K. Junaid, A.E. Abdalla, K.O.A. Abosalif, Z. Ahmed, S. Younas, "COVID-19 and comorbidities: Deleterious impact on infected patients," *Journal of Infection and Public Health*, vol. 13, no. 12, pp. 1833–1839, 2020, doi:10.1016/j.jiph.2020.07.014.

[6] Y. Bai, L. Yao, T. Wei, F. Tian, D.Y. Jin, L. Chen, M. Wang, "Presumed asymptomatic carrier transmission of COVID-19" Jama, vol. 323, no. 14, pp.1406-1407, 2020.

[7] C. Huang, Y. Wang, X. Li, L. Ren, J. Zhao, Y. Hu, L. Zhang, G. Fan, J. Xu, X. Gu, Z. Cheng, T. Yu, J. Xia, Y. Wei, W. Wu, X. Xie, W. Yin, H. Li, M. Liu, Y. Xiao, H. Gao, L. Guo, J. Xie, G. Wang, R. Jiang, Z. Gao, Q. Jin, J. Wang, B. Cao, "Clinical features of patients infected with 2019 novel coronavirus in Wuhan, China," *The Lancet*, vol. 395, no. 10223, pp. 497–506, 2020, doi:10.1016/S0140-6736(20)30183-5.

[8] N. Chen, M. Zhou, X. Dong, J. Qu, F. Gong, Y. Han, Y. Qiu, J. Wang, Y. Liu, Y. Wei, J. Xia, T. Yu, X. Zhang, L. Zhang, "Epidemiological and clinical characteristics of 99 cases of 2019 novel coronavirus pneumonia in Wuhan, China: a descriptive study," *The Lancet*, vol. 395, no. 10223, pp. 507–513, 2020, doi:10.1016/S0140-6736(20)30211-7.

[9] Q. Gao, Y. Hu, Z. Dai, F. Xiao, J. Wang, J. Wu, "The Epidemiological Characteristics of 2019 Novel Coronavirus Diseases (COVID-19) in Jingmen, China," *SSRN Electronic Journal*, vol. 2, no. 8, pp. 113–122, 2020, doi:10.2139/ssrn.3548755.

[10] M. Fathi, K. Vakili, F. Sayehmiri, A. Mohamadkhani, M. Hajiesmaeili, M. Rezaei-Tavirani, O. Eilami, "The prognostic value of comorbidity for the severity of COVID-19: A systematic review and meta-analysis study," PloS one, vol. 16, no. 2, p.e0246190, 2021.

[11] X. Yu, Y. Zhao, Y. Yang, W. He, N. Yang, F. Su, J. Zhu, Z. Zhu, "The magnetic and electronic properties of Ho6Fe23−xCox (x = 0, 1, 2, 3)," *Journal of Magnetism and Magnetic Materials*, vol. 597, , 2024, doi:10.1016/j.jmmm.2024.172029.

[12] B. Wang, R. Li, Z. Lu, Y. Huang, "Does comorbidity increase the risk of patients with covid-19: Evidence from meta-analysis," *Aging*, vol. 12, no. 7, pp. 6049–6057, 2020, doi:10.18632/AGING.103000.

[13] P. Qiu, Y. Zhou, F. Wang, H. Wang, M. Zhang, X. Pan, Q. Zhao, J. Liu, "Clinical characteristics, laboratory outcome characteristics, comorbidities, and complications of related COVID-19 deceased: a systematic review and meta-analysis," *Aging Clinical and Experimental Research*, vol. 32, no. 9, pp. 1869–1878, 2020, doi:10.1007/s40520-020-01664-3.

[14] A. Baradaran, M.H. Ebrahimzadeh, A. Baradaran, A.R. Kachooei, "Prevalence of comorbidities in COVID-19 patients: A systematic review and meta-analysis," *Archives of Bone and Joint Surgery*, vol. 8, no. SpecialIssue, pp. 247–255, 2020, doi:10.22038/abjs.2020.47754.2346.

[15] A. Zaenab, V. Jose, C. J. Cynthia, Z. Yousuf, M. Claudia, S. Hamed, "The Effects of Co-morbidities on COVID-19 Patients Admitted to the Hospital," Fam Med Med Sci Res 10:2, 2021, doi: 10.35248/2327-4972.21.10.261.

[16] WHO Coronavirus (COVID-19) Dashboard (no date) Who.int. Available at: https://covid19.who.int/ (Accessed: June 22, 2021).

[17] A. Clark, M. Jit, C. Warren-Gash, B. Guthrie, H.H.X. Wang, S.W. Mercer, C. Sanderson, M. McKee, C. Troeger, K.L. Ong, F. Checchi, P. Perel, S. Joseph, H.P. Gibbs, A. Banerjee, R.M. Eggo, E.S. Nightingale, K. O'Reilly, T. Jombart, W.J. Edmunds, A. Rosello, F.Y. Sun, K.E. Atkins, N.I. Bosse, S. Clifford, T.W. Russell, A.K. Deol, Y. Liu, S.R. Procter, et al., "Global, regional, and national estimates of the population at increased risk of severe COVID-19 due to underlying health conditions in 2020: a modelling study," *The Lancet Global Health*, vol. 8, no. 8, pp. e1003–e1017, 2020, doi:10.1016/S2214-109X(20)30264-3.

[18] M.F. Beckman, F.B. Mougeot, J.L.C. Mougeot, "Comorbidities and susceptibility to covid-19: A generalized gene set data mining approach," *Journal of Clinical Medicine*, vol. 10, no. 8, 2021, doi:10.3390/jcm10081666.

[19] S. Aktar, A. Talukder, M.M. Ahamad, A.H.M. Kamal, J.R. Khan, M. Protikuzzaman, N. Hossain, A.K.M. Azad, J.M.W. Quinn, M.A. Summers, T. Liaw, V. Eapen, M.A. Moni, "Machine learning approaches to identify patient comorbidities and symptoms that increased risk of mortality in covid-19," *Diagnostics*, vol. 11, no. 8, pp. 1–18, 2021, doi:10.3390/diagnostics11081383.

[20] B. Chakrabarty, D. Das, G. Bulusu, A. Roy, "Network-Based Analysis of Fatal Comorbidities of COVID-19 and Potential Therapeutics," *IEEE/ACM Transactions on Computational Biology and Bioinformatics*, vol. 18, no. 4, pp. 1271–1280, 2021, doi:10.1109/TCBB.2021.3075299.

[21] J. Piñero, Á. Bravo, N. Queralt-Rosinach, A. Gutiérrez-Sacristán, J. Deu-Pons, E. Centeno, J. García-García, F. Sanz, L.I. Furlong, "DisGeNET: A comprehensive platform integrating information on human disease-associated genes and variants," *Nucleic Acids Research*, vol. 45, no. D1, pp. D833–D839, 2017, doi:10.1093/nar/gkw943.

[22] J.S. Amberger, C.A. Bocchini, F. Schiettecatte, A.F. Scott, A. Hamosh, "OMIM.org: Online Mendelian Inheritance in Man (OMIM®), an Online catalog of human genes and genetic disorders," *Nucleic Acids Research*, vol. 43, no. D1, pp. D789–D798, 2015, doi:10.1093/nar/gku1205.

[23] M.J. Landrum, J.M. Lee, M. Benson, G. Brown, C. Chao, S. Chitipiralla, B. Gu, J. Hart, D. Hoffman, J. Hoover, W. Jang, K. Katz, M. Ovetsky, G. Riley, A. Sethi, R. Tully, R. Villamarin-Salomon, W. Rubinstein, D.R. Maglott, "ClinVar: Public archive of interpretations of clinically relevant variants," *Nucleic Acids Research*, vol. 44, no. D1, pp. D862–D868, 2016, doi:10.1093/nar/gkv1222.

[24] E.M. Ramos, D. Hoffman, H.A. Junkins, D. Maglott, L. Phan, S.T. Sherry, M. Feolo, L.A. Hindorff, "Phenotype-genotype integrator (PheGenI): Synthesizing genome-wide association study (GWAS) data with existing genomic resources," *European Journal of Human Genetics*, vol. 22, no. 1, pp. 144–147, 2014, doi:10.1038/ejhg.2013.96.

[25] M. K. Singh, A. Mobeen, A. Chandra, S. Joshi, S. Rama-chandran, "A meta-analysis of comorbidities in COVID-19: Which diseases increase the susceptibility of SARS-CoV-2 infection?," *Computers in biology and medicine*, 130, p.104219, 2021.

[26] J.L. Atkins, J.A.H. Masoli, J. Delgado, L.C. Pilling, C.L. Kuo, G.A. Kuchel, D. Melzer, "Preexisting Comorbidities Predicting COVID-19 and Mortality in the UK Biobank Community Cohort," *Journals of Gerontology - Series A Biological Sciences and Medical Sciences*, vol. 75, no. 11, pp. 2224–2230, 2020, doi:10.1093/gerona/glaa183.

[27] S. Satu, I. Khan, R. Rahman, K.C. Howlader, S. Roy, S.S. Roy, J.M.W. Quinn, M.A. Moni, "Diseasome and comorbidities complexities of SARS-CoV-2 infection with common malignant diseases," *Briefings in Bioinformatics*, vol. 22, no. 2, pp. 1415–1429, 2021, doi:10.1093/bib/bbab003.

[28] M.E. Dolan, D.P. Hill, G. Mukherjee, M.S. McAndrews, E.J.

Chesler, J.A. Blake, "Investigation of COVID-19 comorbidities reveals genes and pathways coincident with the SARS-CoV-2 viral disease," *Scientific Reports*, vol. 10, no. 1, pp. 1–11, 2020, doi:10.1038/s41598-020-77632-8.

[29] J. Yang, Y. Zheng, X. Gou, K. Pu, Z. Chen, Q. Guo, R. Ji, H. Wang, Y. Wang, Y. Zhou, "Prevalence of comorbidities and its effects in coronavirus disease 2019 patients: A systematic review and meta-analysis," *International Journal of Infectious Diseases*, vol. 94, , pp. 91–95, 2020, doi:10.1016/j.ijid.2020.03.017.

[30] B. Thakur, P. Dubey, J. Benitez, J.P. Torres, S. Reddy, "OPEN A systematic review and meta - analysis of geographic differences in comorbidities and associated severity and mortality among individuals with COVID - 19," *Scientific Reports*, pp. 1–13, 2021, doi:10.1038/s41598-021-88130-w.

[31] W. Poole, D.L. Gibbs, I. Shmulevich, B. Bernard, T.A. Knijnenburg, "Combining dependent P- values with an empirical adaptation of Brown ' s method," no. 2002, pp. 430–436, 2016, doi:10.1093/bioinformatics/btw438.

[32] Q. Li, J. Ding, "Fisher ' s method of combining dependent statistics using generalizations of the gamma distribution with applications to genetic pleiotropic associations," pp. 284–295, 2014, doi:10.1093/biostatistics/kxt045.

[33] D. V Zaykin, L.A. Zhivotovsky, P.H. Westfall, B.S. Weir, "Truncated Product Method for Combining P-Values," vol. 185, no. November 2000, pp. 170–185, 2002, doi:10.1002/gepi.0042.

[34] N.A. Heard, P. Rubin-delanchy, "Choosing Between Methods of Combining p -values arXiv : 1707 . 06897v4 [stat . ME] 14 Dec 2017," pp. 1–13, 2017.

[35] L.H.C. Tippett, "The methods of statistics," The Meth-ods of Statistics, pp.222, ref. 66, 1931.

[36] V. Vovk, S.T. Oct, "Combining p-values via averaging," 2019.

[37] D. V Zaykin, "Optimally weighted Z -test is a powerful method for combining probabilities in meta-analysis," vol. 24, , pp. 1836–1841, 2011, doi:10.1111/j.1420-9101.2011.02297.x.

[38] M.C. Whitlock, "Combining probability from independent tests : the weighted Z -method is superior to Fisher ' s approach," vol. 18, , pp. 1368–1373, 2005, doi:10.1111/j.1420-9101.2005.00917.x.

[39] F. Solmi, P. Onghena, "Combining p-values in replicated single-case experiments with multivariate outcome," vol. 24, , pp. 607–633, 2014.

[40] V.C. Tests, "Combining P Values to Get More Power," 2005, doi:10.1002/0470011815.b2a15181.

[41] Z. Chen, W. Yang, Q. Liu, J.Y. Yang, J. Li, M.Q. Yang, "A new statistical approach to combining p-values using gamma distribution and its application to genome-wide association study," vol. 15, no. Suppl 17, pp. 1–7, 2014.

[42] T.P. Speed, B.M. Bolstad, R.A. Irizarry, M. Astrand, "A comparison of normalization methods for high density oligonucleotide array data based on variance and bias," vol. 19, no. 2, pp. 185–193, 2003.

[43] C.W.M. Law, "Precision weights for gene expression analysis (Doctoral dissertation)," 2013.

[44] N.K. Podder, S. Babu, S. Omit, P.C. Shill, H.K. Rana, "Genetic Effects of Covid 19 on the Development of Neurodegenerative Diseases," no. December 2021, pp. 17–19, 2022.

[45] S. Davis, P.S. Meltzer, "BIOINFORMATICS APPLICATIONS NOTE GEOquery : a bridge between the Gene Expression Omnibus (GEO) and BioConductor," vol. 23, no. 14, pp. 1846–1847, 2007, doi:10.1093/bioinformatics/btm254.

[46] G.K. Smyth, "Limma : Linear Models for Microarray Data," no. 2005, pp. 397–420.

[47] T. Uniform, M. Approximation, I. Matrix, L. Rcpp, "Package ' umap ,'" pp. 1–7, 2023.

[48] F. Shahabinezhad, P. Mosaddeghi, M. Negahdaripour, M. Farahmandnejad, M.J. Taghipour, M. Moghadami, N. Nezafat, S.M. Masoompour, "Therapeutic approaches for COVID-19 based on the dynamics of interferon- mediated immune responses," no. March, 2020, doi:10.20944/preprints202003.0206.v2.

[49] H. Rahman, H.K. Rana, S. Peng, X. Hu, C. Chen, J.M.W. Quinn, M.A. Moni, "Bioinformatics and machine learning methodologies to identify the effects of central nervous system disorders on glioblastoma progression Bioinformatics and machine learning methodologies to identify the effects of central nervous system disorders on glio," no. January, 2021, doi:10.1093/bib/bbaa365.

[50] Z. Nain, H.K. Rana, P. Liò, S. Mohammed, S. Islam, M.A. Summers, "Pathogenetic profiling of COVID-19 and SARS-like viruses," vol. 22, no. 2, pp. 1175–1196, 2021, doi:10.1093/bib/bbaa173.

[51] G. V Glinsky, "Impacts of genomic networks governed by human-specific regulatory sequences and genetic loci harboring fixed human-specific neuro-regulatory single nucleotide mutations on phenotypic traits of modern humans," *Chromosome Research*, vol.28, pp. 331–354, 2020, doi: 10.1007/s10577-020-09639-w

[52] P. Mosaddeghi, F. Shahabinezhad, Z. Dehghani, M. Farahmandnejad, M. J. Taghipour, M. Moghadami, N. Nezafat, S. M. Masoompour, M. Negahdaripour, "Therapeutic Approaches for COVID-19 Based on the Interferon-mediated Immune Responses", *Current Signal Transduction Therapy*, vol. 16, no. 1. 2021, doi:10.2174/1574362416666210120104636

[53] M. V Kuleshov, M.R. Jones, A.D. Rouillard, N.F. Fernandez, Q. Duan, Z. Wang, S. Koplev, S.L. Jenkins, K.M. Jagodnik, A. Lachmann, M.G. Mcdermott, C.D. Monteiro, W. Gundersen, A. Ma, "Enrichr : a comprehensive gene set enrichment analysis web server 2016 update," vol. 44, no. May, pp. 90–97, 2016, doi:10.1093/nar/gkw377.

[54] A.M. Khan, Z. Ajmal, M. Raval, E. Tobin,"Con-current diagnosis of acute myeloid leukemia and COVID-19: a man-agement challenge," *Cureus*, vol. 12, no. 8, 2020, doi:10.7759/cureus.9629

[55] H.A. Tehrani, M. Darnahal, S.A. Nadji, S. Haghighi, "COVID-19 re-infection or persistent infection in patient with acute myeloid leukaemia M3 : a mini review," *New Microbes and New Infections*, vol. 39, , pp. 100830, 2021, doi:10.1016/j.nmni.2020.100830.

[56] A.O. Brien, J. Campling, H. Goodman, C.L. Chang, "Respirology Case Reports presentation and management implications," vol. 8, , pp. 1–5, 2020, doi:10.1002/rcr2.650.

[57] M. Gavillet, J.C. Klappert, O. Spertini, S. Blum, "Acute leukemia in the time of COVID-19," *Leukemia research*, 92, p.106353, 2020.

[58] J. Sarkis, R. Samaha, "Bladder cancer during the COVID-19 pandemic : the calm before the storm ?," Future Science, vol. 6, no. 8, pp. 13–15, 2020, doi: 10.2144/fsoa-2020-0101

[59] The experience of UK patients with bladder cancer during the COVID-19 pandemic : a survey-based snapshot, pp. 179–181, 2021, doi:10.1111/bju.15287.

[60] L. Di Filippo, R. De Lorenzo, E. Cinel, E. Falbo, M. Ferrante, M. Cilla, S. Martinenghi, G. Vitali, E. Bosi, A. Giustina, P. Rovere-Querini, C. Conte, "Weight trajectories and abdominal adiposity in COVID-19 survivors with overweight/obesity," *International Journal of Obesity*, vol. 45, no. 9, pp. 1986–1994, 2021, doi:10.1038/s41366-021-00861-y.

[61] H.S.J. Chew, V. Lopez, "Global impact of covid-19 on weight and weight-related behaviors in the adult population: A scoping review," *International Journal of Environmental Research and Public Health*, vol. 18, no. 4, pp. 1–32, 2021, doi:10.3390/ijerph18041876.

[62] M. Shih, B. Swearingen, R. Rhee, N. York, "Since January 2020 Elsevier has created a COVID-19 resource centre with free information in English and Mandarin on the novel coronavirus

COVID- 19 . The COVID-19 resource centre is hosted on Elsevier Connect , the company ' s public news and information ," no. January, 2020.

[63] M.H. Syed, M. Wheatcroft, D. Marcuzzi, H. Hennessey, M. Qadura, "Management of a mycotic aneurysm in a patient with COVID-19: A case report," *Medicina (Lithuania)*, vol. 57, no. 6, pp. 1–7, 2021, doi:10.3390/medicina57060620.

[64] I. Tsimafeyeu, G. Alekseeva, M. Berkut, A. Nosov, I. Myslevtsev, A. Andrianov, A. Semenov, P. Borisov, R. Zukov, V. Goutnik, S. Savchuk, M. Volkova, M. Mukhina, "COVID-19 in Patients With Renal Cell Carcinoma in the Russian Federation," *Clinical Genitourinary Cancer*, vol. 19, no. 2, pp. e69–e71, 2021, doi:10.1016/j.clgc.2020.07.007.

[65] M. Mihalopoulos, N. Dogra, N. Mohamed, K. Badani, N. Kyprianou, "COVID-19 and Kidney Disease: Molecular Determinants and Clinical Implications in Renal Cancer," *European Urology Focus*, vol. 6, no. 5, pp. 1086–1096, 2020, doi:10.1016/j.euf.2020.06.002.

[66] N. Zaki, H. Alashwal, S. Ibrahim, "Association of hypertension, diabetes, stroke, cancer, kidney disease, and high-cholesterol with COVID-19 disease severity and fatality: A systematic review," *Diabetes and Metabolic Syndrome: Clinical Research and Reviews*, vol. 14, no. 5, pp. 1133–1142, 2020, doi:10.1016/j.dsx.2020.07.005.

[67] C. Sardu, G. Gargiulo, G. Esposito, G. Paolisso, R. Marfella, "Impact of diabetes mellitus on clinical outcomes in patients affected by Covid-19," *Cardiovascular Diabetology*, vol. 19, no. 1, pp. 4–7, 2020, doi:10.1186/s12933-020-01047-y.

[68] L. Fang, G. Karakiulakis, M. Roth, "Are patients with hypertension and diabetes mellitus at increased risk for COVID-19 infection?," *The Lancet Respiratory Medicine*, vol. 8, no. 4, pp. e21, 2020, doi:10.1016/S2213-2600(20)30116-8.

[69] S. Lim, J.H. Bae, H.S. Kwon, M.A. Nauck, "COVID-19 and diabetes mellitus: from pathophysiology to clinical management," *Nature Reviews Endocrinology*, vol. 17, no. 1, pp. 11–30, 2021, doi:10.1038/s41574-020-00435-4.

[70] S.B. Sen Omit, S. Akhter, H.K. Rana, A.R.M.M.H. Rana, N.K. Podder, M.I. Rakib, A. Nobi, "Identification of Comorbidities, Genomic Associations, and Molecular Mechanisms for COVID-19 Using Bioinformatics Approaches," *BioMed Research International*, vol. 2023, no. December 2019, 2023, doi:10.1155/2023/6996307.

[71] A.F. Kantor, P. Hartge, R.N. Hoover, A.S. Narayana, J.W. Sullivan, J.F. Fraumeni, "Urinary tract infection and risk of bladder cancer," *American Journal of Epidemiology*, vol. 119, no. 4, pp. 510–515, 1984, doi:10.1093/oxfordjournals.aje.a113768.

[72] T. Brown, R. Slack, L. Rushton, "Occupational cancer in Britain: Urinary tract cancers: Bladder and kidney," *British Journal of Cancer*, vol. 107, no. S1, pp. S76–S84, 2012, doi:10.1038/bjc.2012.121.

[73] C.D.S. Costa, E.M. Steele, M.A. Leite, F. Rauber, R.B. Levy, C.A. Monteiro, "Body weight changes in the NutriNet Brasil cohort during the covid-19 pandemic," *Revista de Saude Publica*, vol. 55, , pp. 1–5, 2021, doi:10.11606/S1518-8787.2021055003457.

[74] D.C. Van Duijvenbode, M.J.M. Hoozemans, M.N.M. Van Poppel, K.I. Proper, "The relationship between overweight and obesity, and sick leave: A systematic review," *International Journal of Obesity*, vol. 33, no. 8, pp. 807–816, 2009, doi:10.1038/ijo.2009.121.

[75] L. Smith, J. Taylor, A. Lewis, "Tailored Medication Regimens for Patients with Comorbidities: A Review," *Journal of Pharmacy Practice*, 32(5), 561–569, 2019.

[76] A. L. Jones, P. S. Duggan, S. O'Brien, "Comorbidities and Mental Health Disorders: The Need for Integrated Care," *Irish Medical Journal*, 113(6), 89, 2020.

[77] A. Marengoni, S. Angleman, R. Melis, F. Mangialasche, A. Karp, A. Garmen, B. Meinow, L. Fratiglioni, "Aging with multimorbidity: A systematic review of the literature," *Ageing Research Reviews*, vol. 10, no. 4, pp. 430–439, 2011, doi:10.1016/j.arr.2011.03.003.

[78] E. A. Brown, E. Mahanna, F. J. Schiffman, "Comorbidity Assessment in Surgical Patients," *Anesthesiology Clinics*, 36(1), 1–14, 2018.